19. Modern Fuel Cell Testing Laboratory

Jean St-Pierre, Michael Angelo, Keith Bethune, Jack Huizingh, Tatyana Reshetenko, Mebs Virji, Yunfeng Zhai

Elements constituting a fuel cell laboratory are succinctly discussed using the experience developed at the Hawaii Sustainable Energy Research Facility. The information is expected to be useful to organizations with a desire to create or improve a fuel cell laboratory in view of the recent and anticipated fuel cell commercialization activities. Topics discussed cover a wide range with an emphasis on differentiating aspects from other types of laboratories including safety, fuel cell and test equipment, and methods used to characterize fuel cells. The use of hydrogen, oxygen and specifically introduced chemical species, and the presence of high voltages and electrical short risks constitute the most prominent hazards. Reactant purity, cleaning, test station control including data acquisition, and calibration are the most important considerations to ensure fuel cell characterization data quality. Cleanliness is also an important consideration for the fuel cell assembly and integration into the test station. The fuel cell assembly also needs to be verified for faults. Fuel cells need to be conditioned for optimum performance before a purposefully designed test plan is implemented. Many fuel cell diagnostic methods are available but novel techniques are still needed in many areas including through plane temperature distribution, stack diagnostics and mass transfer properties. The emphasis is given to commonly and sparingly used electrochemical techniques. In situ techniques include polarization, impedance spectroscopy, voltammetry and current distribution over the active area. Ex situ techniques include the rotating ring-disc electrode and the membrane conductivity cell. Other nonelectrochemical techniques are also useful to understand fuel cell behavior and include the analysis of reactant streams and condensed water, and spectroscopic measurements in combination with electrochemical cells (spectroelectrochemical cells).

19.1 Fuel Cell Laboratory Evolution

Developments in fuel cell technology have recently culminated with the commercial release of cars. This evolution as well as progress in similar technologies is expected to continue and will affect the fuel cell laboratory in several ways. An expanding demand for a specialized fuel cell knowledgeable work force will redefine the scope and spreading of fuel cell laboratories and bring to the forefront specific safety risks.

19.1.1 Background

The development of fuel cell technology has significantly progressed during the last few years [19.1]. Fuel cell forklifts are currently being demonstrated and are claimed to already be cost effective in comparison to batteries. Fuel cell cars are also being demonstrated with the anticipation that they will be commercialized on a limited basis during 2015. Fuel cell demonstrations are not limited to motive applications and also include generators for homes. This situation implies that fuel cell laboratories have concurrently been established at companies, national laboratories and universities to sustain research and development activities. In view of the progress achieved and anticipated in fuel cell technology deployment, it is a worthwhile endeavor to reflect on future fuel cell laboratory needs. The education and empowerment of a technically knowledgeable installation, maintenance, diagnosis and repair workforce represents such an example that is supported by a predicted increase in the fuel cell related workforce [19.2]. The resurgence of interest in the development of flow batteries [19.3] for grid energy storage to enhance the penetration of intermittent power sources (solar, wind) represents another incentive to reevaluate future fuel cell laboratory needs. Flow batteries are similar to fuel cells with liquid rather than gaseous reactant streams circulating through the device. The technology has evolved towards a similar fuel cell membrane-electrode assembly (MEA) and bipolar plate design to concurrently enable operation at higher current densities and decrease cost (United States patent application 2012/0258345). A fast recharge is also possible by replacing the depleted electrolytes in the storage tanks rather than by reconstituting the original redox species by reversing the current flow as with a secondary battery recharge.

A comprehensive discussion of a fuel cell laboratory has not been found although examples for other types of laboratories are available. A report recently appeared for an analytical laboratory focusing on measurement techniques [19.4]. However, many fuel cell laboratory elements have already been separately discussed including education material [19.5, 6], standardization of measurement methods [19.7–9], and the relationship between laboratory and application measurements [19.10]. Several measurement method reviews have also appeared [19.11]. Mathematical modeling is also considered as a valid laboratory method in cases where measurements are not possible, are difficult due to space or other constraints, or are expected to create significant artifacts. For instance, a model is needed to generate the current distribution across flow field channels from potential sensing probes (submillimeter dimension [19.12]) and assess the effects associated with the presence of a foreign cation in a membrane [19.13, 14]. In turn, fuel cell measurements are necessary for model validation and to gain confidence in their predictive capabilities. Other important elements include safety (hydrogen, high current electrical shorts, etc.), personnel and fuel cell stack or system fabrication capabilities.

Staffing and Education

The need for education and personnel training cannot be overemphasized especially to increase fuel cell laboratory efficiency and standing. The current Hawaii Sustainable Energy Research Facility (HiSERF) workforce is composed of scientists and engineers with diverse characteristics (age, race, sex, ethnicity, nationality, culture, etc.). Such a group composition has been discussed as one of the elements fostering creativity [19.15]. Interestingly, the group includes a technician who has not received fuel cell training from an academic institution. This statement is symptomatic of a larger issue that has already been identified. There is a significant gap in education about hydrogen and fuel cell technologies below the university level (Fig. 19.1) especially in view of the anticipated increase in the fuel cell related workforce [19.2]. A few topics (Fig. 19.1) are especially relevant to the present discussion including fuel cells, hydrogen production and storage, chemistry, physics and engineering. The inclusion of new technology in public education is important to manage expectations and facilitate technology diffusion (sustainable growth) and commercialization (equipment maintenance). For a fuel cell laboratory, specifically trained technicians would free current fuel cell operators, scientists and engineers, from their duties, allowing them to devote more of their time to their core activities:

- Experimental plan development
- Data analysis
- Reporting functions (presentations, publications, patents) and
- Proposal preparation.

The need for technicians varies with the type of organization. At universities, student education and limited resources constrain the number of technicians whereas at commerce-driven organizations, better resources and the necessity for an optimum efficiency favor a larger technician contingent.

The sustainability trend represents a wider scope opportunity to integrate fuel cell technology into the education curriculum [19.18]. Already, many exam-

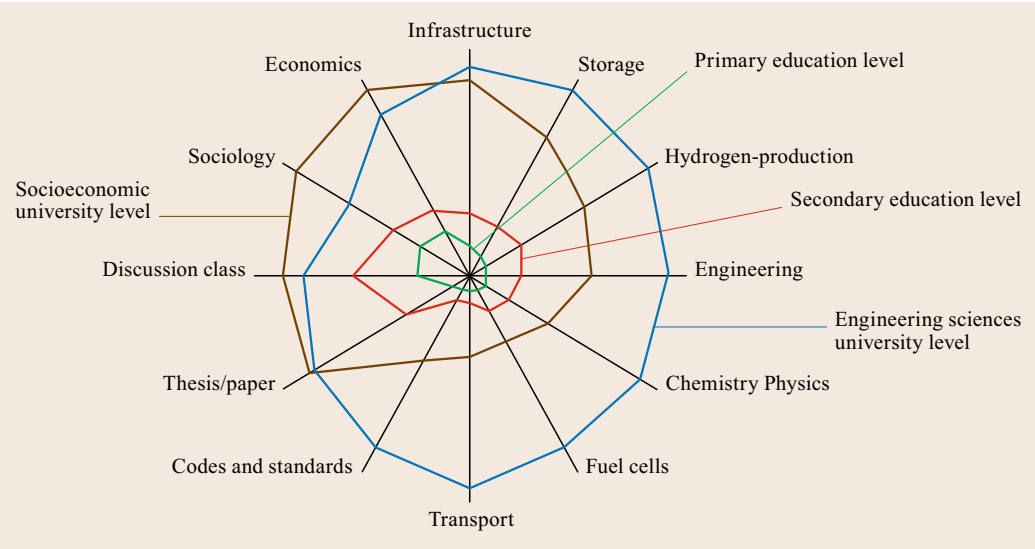

Fig. 19.1 Hydrogen technologies penetration into educational program curricula (after [19.16])

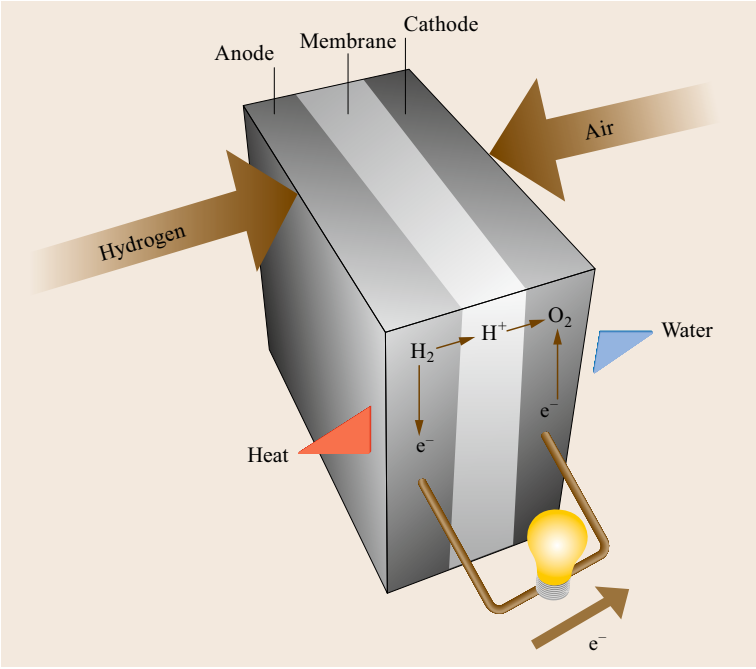

Fig. 19.2 PEMFC operation diagram illustrating key components, reactions ($O_2 + 4H^+ + 4e^- \rightarrow 2H_2O$, $2H_2 \rightarrow 4H^+ + 4e^-$) and output (after [19.17])

ples of fuel cell related material have been proposed to help instructors and teachers [19.19] including the photo-production of hydrogen by algae fed to a proton exchange membrane fuel cell (PEMFC [19.20]), bacteria fuel cells [19.21], a borohydride (hydrogen source) fuel cell [19.5] and a thin layer fuel cell [19.6]. Present educational efforts also mean that future scientists and engineers will be sensitized at a much younger age to fuel cell and related technologies. The impact of this statement on future scientists and engineers' effectiveness remains to be evaluated. Therefore, there is a need to define a clear role for fuel cell laboratories in the educational effort. Also, a complete compendium of all fuel cell laboratory-relevant elements would be valuable to foster the integration of new organizations interested in developing fuel cell technology, evaluating or planning strategic expansions of existing facilities, and identifying gaps.

Key information for many fuel cell laboratory elements is summarized and referenced. Focus will be

given to the PEMFC (Fig. 19.2) to limit the scope. The other main fuel cell technology of commercial interest, the solid oxide fuel cell (SOFC, Fig. 19.2), is expected to still largely benefit from the content by inciting discussions despite distinctive differences associated with higher temperatures (an additional safety risk) and the use of ceramic rather than polymer and other materials. Areas that require improvement are also identified. The information is largely representative of HiSERF with a scope including PEMFC material research, and cell, stack and system characterization. For instance, key electrochemical methods are illustrated with data obtained at HiSERF. The information represents an overview that cannot be comprehensive at the detailed level due in part to the large scope considered but it is hoped that this initial effort will be sufficient to achieve the stated objectives and generate further discussion.

19.1.2 Fuel Cell Laboratory Overview

A fuel cell laboratory is in many respects similar to other laboratories. A fuel cell laboratory is still populated by scientists, engineers and technicians that are concerned with safety aspects including waste disposal, safety devices such as fume hoods and showers, chemicals, analytical equipment, and so on. There are also key differences as high purity fuels and oxidants need to be provided (hydrogen, air or O_2) creating specific safety challenges. In addition, fuel cells need to be assembled, tested and disassembled. These key differences are discussed in more detail in subsequent sections:

- Safety and test stations
- Fuel cell/stack, components and assembly
- Testing and diagnostic techniques.

19.2 Safety and Test Stations

Safety aspects associated with fuel cell technology cannot be overemphasized in view of the negative impact a hydrogen related incident, such as the Hindenburg airship in 1937, could have on public perception. From that standpoint, the fuel cell laboratory infrastructure as well as test station design is of particular importance to minimize safety risks. The test station design is also important to ensure fuel cell characterization is possible under a practical range of conditions and data are acquired and stored at a sufficient rate.

19.2.1 Safety

It is first emphasized that general laboratory safety procedures are assumed to be implemented. The most important additional safety risks associated with a fuel cell laboratory are related to chemicals, reactants, contaminants and tracers, and electricity with high voltages and currents. Hydrogen, oxygen, contaminant and tracer species, electrical shorts and high voltages are discussed with the recognition that other concerns may exist especially if other fuel cell technologies gain prominence. For instance, other oxidants and fuels have been proposed including hydrazine [19.22], dimethyl ether [19.23], peroxide [19.24] and borohydride [19.25] that require different handling and safety procedures. Safety is first addressed at the facility planning stage, which is subsequently followed up by a change management procedure to ensure modifications are made in response to evolutionary trends (new employees, change in research focus, etc.).

Facility Planning, Codes and Regulations

Research and related experimental activities are uncertain in nature and necessitate particular attention to safety and environmental concerns. Safe practices are essential for the protection of personnel, equipment, research integrity and environment. Planning and design of a fuel cell testing laboratory begins with a scope of work, which defines the type and scale of research and testing activities to be conducted, the amount of hazardous materials that might be encountered and the potential risks to personnel and equipment. The scope of work is followed by a sound safety plan that reflects thoughtful consideration of the identification and analysis of safety vulnerabilities (primary and secondary failure modes ranging from benign to catastrophic), hazards prevention, risks mitigation, and effective organization and communication. The safety plan also recognizes the human error factors, equipment life and limitations and the planned or unforeseen changes that occur over the life of the laboratory.

Many sources of information are readily available to support the development and implementation of a safety plan, ranging from promoting organizations and funding agencies (United States Department of Energy, Fuel Cell and Hydrogen Energy Association, etc.) to regulatory organizations codes and standards (National Fire Protection Association, American Society of Mechanical Engineers, American National Standards Institute, International Electrotechnical Commission, Compressed Gas Association, etc.) and safety organizations (Occupational Safety and Health Administration,

etc.). In addition to the wealth of available information, private companies, public agencies, academic institutions and experienced consultants and personnel represent other sources with relevant experience of use for the planning, construction and operation process. Only specific safety risks associated with a fuel cell testing laboratory are discussed in the following sections.

Hydrogen

Hydrogen is considered a likely fuel because it can be produced from water by electrolysis and its consumption in a fuel cell results in the formation of water thus reconstituting the initial stock. Hydrogen is also produced by methane steam reforming. Hydrogen diffuses through solid materials due to its small molecular size. Leaks are also possible near fuel cell and other piping connections. The accumulation of hydrogen in open spaces near ceilings (low vapor density of 0.1 in comparison to air [19.26]) needs to be prevented because little energy is needed to ignite it (low minimum ignition energy of 0.017 mJ [19.26]). This is especially important for leaks because hydrogen warms with a decrease in pressure above the inversion temperature of $\approx 200\,\mathrm{K}$ (Joule–Thomson coefficient) and may spontaneously ignite. Mitigation of the risks is achieved through material selection, detection by sensors linked to an alarm and control system to initiate shutdown procedures and design by adequate ventilation and dilution below the 4% volumetric flammable limit [19.26]. Reactant streams are usually humidified and heating tapes controlled by a thermocouple are used to keep the water in vapor form. Convenient and flexible polymer tubing should not be used as the heating capacity of the heating tapes is sufficient to melt the polymer and create a leak in the event temperature control is lost. The use of an odorant to facilitate leak detection is not recommended as fuel cell operation is likely to be adversely affected.

Other hydrogen sources such as liquid hydrogen or onsite generators (water electrolyzer with additional closed space) add supplementary hazards. Liquid hydrogen is sufficiently cold (boiling point of $-252\,^{\circ}\mathrm{C}$ [19.26]) to create solid oxygen and nitrogen, thermal stresses in system materials and embrittlement of metallic components with hydrogen accumulation in the material microvoids. These risks are minimized by controlled cool down procedures and material selection. A limited liquid hydrogen spill will rapidly disperse but a continuous spill creates an expanding low cloud of dense hydrogen vapors (cold hydrogen is denser than air) that may explode over water. Detailed safety information is readily available (for example, National Fire Protection Association (NFPA) 2 and 55 codes [19.27, 28]).

Oxygen

Air is the preferred oxidant for most applications because it does not need to be stored onboard a system with the exception of air independent devices such as space and underwater vehicles. Oxygen is generally used for diagnostic purposes. A first order estimate of the mass transport overpotentials, gas phase and ionomer phase contributions, is obtained with the sequential use of different oxidant compositions (O_2, 21% O_2/79% He and air [19.29, 30]). This aspect will be more extensively discussed in Sect. 19.4.2. However, additional safety precautions are necessary because combustible material deposits (oils for instance) can ignite as a result of a sudden O_2 compression (gas line pressurization). Gas line and fuel cell materials need to be properly selected and cleaned for O_2 service. Pressurization procedures need to be changed by first pressurizing with an inert gas and subsequently switching to O_2. For long-term O_2 service (life tests), it is advisable to add redundancies for fire detection. Thermocouples located at the reactant stream and coolant outlets as well as H_2 and O_2 sensors in the reactant stream outlets are useful to detect a membrane failure allowing reactants to mix and combust in the presence of the catalyst. These devices need to be linked to the control software to trigger a test station shutdown. An extensive discussion of design aspects for O_2 use is available [19.31] and courses on O_2 systems design and safety are offered.

Contaminant and Tracer Species

A few reasons justify the injection of species that are not reactants into a fuel cell. Ambient air contains hundreds of contaminants that may adversely affect fuel cell performance [19.32–35]. These contaminants originate from a variety of sources but many are generated by the chemical industry and are organic. The fuel stream also contains contaminants that are equally deleterious to fuel cell performance [19.36]. Their nature and concentration depends on the fuel synthesis process (methane reforming, water electrolysis) and purification cost. Although H_2 fuel contaminants may not necessarily include organic species, contaminants leached or evolved from system materials contain organic and other species [19.37]. Finally, tracer species are injected to measure residence time distributions and evaluate fuel cell flow behavior and liquid water content [19.38, 39]. These tracers are commonly colored or radioactive species [19.40]. Contaminants and tracers are usually in low concentrations. Higher contaminant concentrations are used for fuel cell tests to accelerate degradation and minimize the confounding effect of other degradation mechanisms. The toxicity of the reactant gas streams is therefore a con-

cern [19.32–34] and is partially mitigated by using surrogate molecules with the same functionalities but with slightly different structures or less toxic alternatives. It is assumed that the substitute molecules with lower toxicity similarly behave in a fuel cell as the original molecule or are as easily detectable (tracers). The material safety data sheet (MSDS) or equivalent needs to be consulted before tests are initiated, which contains safety information including treatment and disposal (Environment Protection Agency and Occupational Safety and Health Administration regulations). Contaminant and tracer species may be restricted or require special shipment procedures. Other considerations include the need to purge the gas before disconnecting a gas cylinder for replacement and cleaning the gas lines after use to limit carry over to subsequent tests.

Electrical Shorts and High Voltages

In a PEMFC, bipolar plates are only separated by a very short distance that corresponds to the membrane thickness ($\approx 25-50\,\mu m$). The risk associated with electrical shorts cannot therefore be ignored. Also, to achieve higher working voltages cells are usually arranged in series in a fuel cell stack. Stacks operating over 100 V can create a significant electrocution risk that can be lethal [19.41]. The requirement for stack compactness and high power densities reduces the number of options available to decrease short circuit risks. Electrical insulation is effective in preventing contact between adjacent bipolar plates with tools such as screwdrivers and operators wearing metallic rings (Occupational Safety and Health Administration lockout/tagout practices and procedures). Electrical insulation is also effective to reduce electrical shocks. Equally thin battery electrodes also prone to electrical short circuits offer another source of inspiration to improve PEMFC designs [19.42]. The safety risk is not only limited to the external surface of the fuel cell. Polymeric membranes are prone to failure and the creation of pinholes bringing both reactant streams into contact [19.43]. The combustion favored by the presence of a catalyst locally raise the temperature [19.44], which may in severe cases be sufficient to melt the polymer and enlarge the pinhole. This situation may be exacerbated by the short circuit risk between both electrodes especially if they are based on a flexible carbon material (felt, cloth). For this specific case, the risk is mitigated by the presence of thermocouples and O_2 or H_2 sensors mentioned in Sect. 19.2.1. However, the effects of a short circuit develop very rapidly [19.45]. Therefore, mitigation measures may not be sufficient to prevent irreversible damage.

19.2.2 Test Stations

Fuel cells require support equipment (balance of plant) to function including an air compressor or blower, reactant humidifiers, a heat exchanger, a voltage converter, an electrical motor and controls (Fig. 19.3). A fuel cell test station fulfills the same functions as the balance of plant but is more sophisticated and able to provide independently controlled and well-characterized operating conditions for research and development purposes. Test stations are available from a variety of commercial suppliers for both single cells and stacks. Test stations may equally be assembled from commercial parts, however data collection and logging can overwhelm a standard personal computer. The test station is interfaced with reactant supplies in the laboratory emphasizing purity aspects and associated piping cleaning requirements. Test station systems control reactant and diagnostic gas selection, flows, humidification and pressure, cell or stack temperature, voltage-current output and data acquisition. Test stations need to be maintained and regularly calibrated. Test stations are supplemented by other diagnostic equipment to complete additional specific measurements (Sect. 19.4.2) such as current-voltage distributions, liquid water content and outlet gas or liquid water composition.

Reactants Supply and Purity

The performance and durability of PEMFCs is affected by the quality of the reactant gases [19.36, 46]. For the hydrogen fuel, numerous methods exist for its production and purification that result in different contaminants and quality levels. The Society of Automotive Engineers (SAE) recently published a hydrogen fuel quality standard for fuel cell vehicles (SAE J2719, Table 19.1). The hydrogen fuel index is specified as 99.97%, although the primary contributors are inert gases, which are only a concern at these levels if recirculation systems are of interest because contaminants accumulate and reach even higher concentrations [19.47]. The other contaminant concentrations such as for ammonia and sulfur species are ≤ 5 ppm (volumetric basis). Many of these low concentration contaminants still have a significant effect on fuel cell performance [19.36] but are below standard gas analysis detection limits. Therefore, the use of a high efficiency purifier such as a palladium membrane or getter-based devices in combination with a sufficiently high purity source ($\geq 99.995\%$) from a proton exchange membrane electrolyzer for example, is highly recommended to eliminate systematic errors.

Air quality varies around the world and most laboratory air is produced on site with a compressor system. The International Organization for Standard-

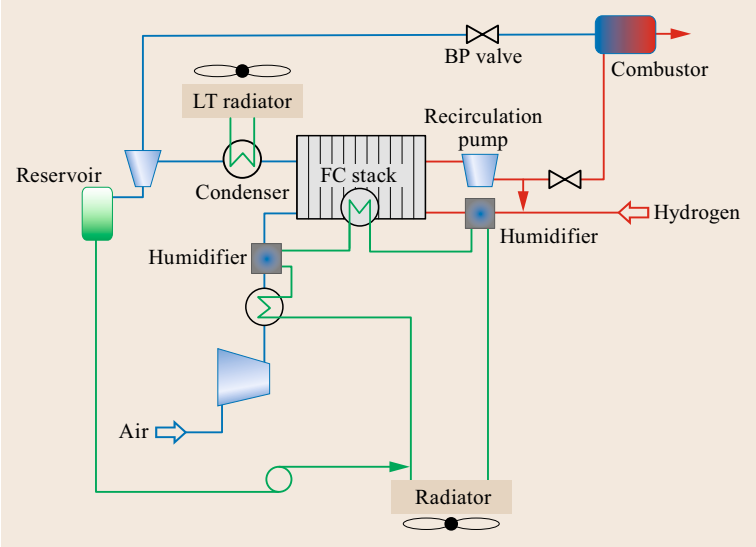

Fig. 19.3 A PEMFC system layout depicting the fuel cell (FC) stack and balance of plant components (BP: bypass, LT: low temperature)

Table 19.1 SAE J2719 hydrogen fuel quality standard

Contaminant	Maximum allowable quantity (ppm by volume unless otherwise specified)
Ammonia	0.1
Carbon dioxide	2
Carbon monoxide	0.2
Formaldehyde	0.01
Formic acid	0.2
Helium	300
Nitrogen and argon	100
Oxygen	5
Particulates	1 µg/l at normal temperature and pressure
Total gases	300
Total halogenated compounds	0.05
Total hydrocarbons	2
Total sulfur compounds	0.004
Water	5

ization (ISO) ISO 8573 series of standards relates to the compressed air quality. ISO 8573-1 describes purity classes that are only distinguished by the maximum oil and water vapor content, and particulate levels. ISO 8573-5 specifies test methods for determining the oil vapor content ($\geq C_6$ hydrocarbons) as well as any organic solvents. ISO 8573-6 specifies test methods for gaseous contaminants consisting of carbon monoxide, carbon dioxide, sulfur dioxide, nitric oxide, nitrogen dioxide and hydrocarbons in the C_1 to C_5 range. However, contaminant level classifications are not included. The most comprehensive classification for ultrahigh purity air quality is contained in the Compressed Gas Association's (CGA) standard CGA G-7.1, Grade J for

Table 19.2 CGA grade J air composition

Species	Concentration (ppm by volume unless otherwise specified)
O_2 (%)	19.5–23.5
Water	1
Carbon monoxide	1
Carbon dioxide	0.5
Total hydrocarbon content as methane	0.5
Halogenated solvents	0.1
Nitrogen dioxide	0.1
Nitrous oxide	0.1
Sulfur dioxide	0.1

specialty air/analytical purposes (Table 19.2). Similar to the SAE standard for hydrogen quality, the maximum limits are very low for the contaminants listed ($\leq$ 1 ppm on a volumetric basis). Trace amounts of contaminants adversely affect fuel cell performance [19.35, 46]. Therefore, the air supply system design needs to surpass the air quality specified in the CGA standard. Table 19.3 describes an air supply and purification system that provides ultrahigh quality air similar to CGA Grade J. Other diagnostic reactant stream gases [19.29, 30] such as nitrogen, helium and oxygen, also need to be of sufficient quality to avoid detrimental effects on fuel cell performance. Thus, high efficiency purification units should also be considered even if research grade gases are purchased.

System Cleaning

The laboratory gas distribution network and PEMFC test stations are composed of piping distribution systems exposed to dry supply gas streams, heated and

Table 19.3 Example of system components for fuel cell laboratory air production

Component (sequentially from upstream)	Description
Oil-free scroll compressor	Initial intake filtration for particles > 10 μm; oil-free compression
Refrigerated dryer	Bulk water vapor removal; gas cooling
Dual stage coalescing filters	Oil and particulate removal for particles > 1 μm (stage 1) and > 0.01 μm (stage 2)
Activated carbon filter	Odor and non-methane hydrocarbon removal
Pressure swing adsorption system	Desiccant for H_2O removal and/or molecular sieve 13X for H_2O and CO_2 removal (achieves < 1 ppm CO_2 and < −70 °C dew point)
Particulate filter	Remove particles from pressure swing adsorption system > 0.01 μm
Mixing tank	Stabilize O_2 concentration swings due to pressure swing adsorption system
Activated carbon filter	Eliminate volatile organic carbons from the coated mixing tank
Semiconductor grade filter	Provides final chemical filtration of acids, bases and organics down to the ppb level

humidified gas streams and deionized water. The selection of piping distribution systems and the test station parts and components materials are first considered to ensure compatibility with gaseous and liquid fluids, and exposure conditions. This step is necessary to prevent contamination issues due to adverse reactions between fluids and materials. For example, metallic corrosion releases ions into the coolant water as well as rust and particulates. Components and assemblies with exposed surfaces need to be cleaned prior to assembly using mechanical and chemical cleaning methods. Several organizations as well as manufacturers provide overview documents for high purity or ultrahigh purity parts design, installation, and cleaning. These guides extend the information contained in CGA (CGA G-4.1, CGA G-5.4, CGA PS-31) and American Society for Testing and Materials International (ASTMI) standards (ASTM A380-06, ASTM G 93-03). For general use fuel cell test stations, material specifications for components do not have to fulfill ultrahigh purity levels such as those required in the semiconductor industry. If contaminants are deliberately introduced into the fuel cell, the system needs to be cleaned before other tests are completed. For that specific case, it is acceptable to at least purge with inert gases under higher temperatures to favor contaminant desorption. In that regard, difficult-to-access dead spaces need to be minimized.

Test Station Control Systems

A fuel cell test system consists of components and subassemblies designed to provide management of the gaseous and liquid fluids being supplied to the fuel cell, to control the electrical output of the fuel cell, and to record and process data from various sensors. The degree of complexity, automation, and dynamic response required depends on the specific application. Station designs range from very basic stations for routine measurements with a limited number of control options (United States Fuel Cell Council document 04-011B) to more complex station designs such as hardware-in-the-loop type stations where fuel cell system components can be simulated and interfaced with an operating stack [19.48, 49], modular test stations allowing for easy exchange of various types of subassemblies [19.50], and even subfreezing stations [19.51]. Figure 19.4 presents a block diagram of the main components and subassemblies that comprise a fuel cell test station.

Gas Selection and Flow Control. The test station gas delivery system provides gas selection, mixing and flow control for various fuel and oxidant mixtures. A basic test station may have only one flow controller for fuel and oxidant delivery. The gas supplied to the flow controller is changed either by switching sources or manually turning valve selectors. Typical test stations have several flow controllers for both the fuel and oxidant mixtures. The number and complexity of the flow controller manifolds depend on the level of flexibility required. Multiple flow controllers are used to create, for example, simulated reformate fuel gas mixtures for testing or oxidant mixtures with different diluent gases for mass transfer studies [19.29, 30]. The turndown ratio is improved by using multiple flow controllers for individual gases to cover a larger range of flow rates. Several types of flow controllers exist. Thermal mass flow controllers are typically used (Brooks Instrument white paper T/021).

Humidification Control. For the majority of PEMFCs especially at the laboratory scale, external humidifiers are used to supply humidified gases and maintain high membrane conductivity [19.52]. A humidification system consists of the humidifier unit as well as heated delivery lines to prevent condensation in the tubing interconnect between the cell and the humidifier. Several types of humidifiers have been utilized in test stations including bubbler dew point saturators, steam injection, flash vaporization, membranes, packed bed/spray chamber contact humidifiers, and so on. The humidifier selection depends on the gas composition, heating and

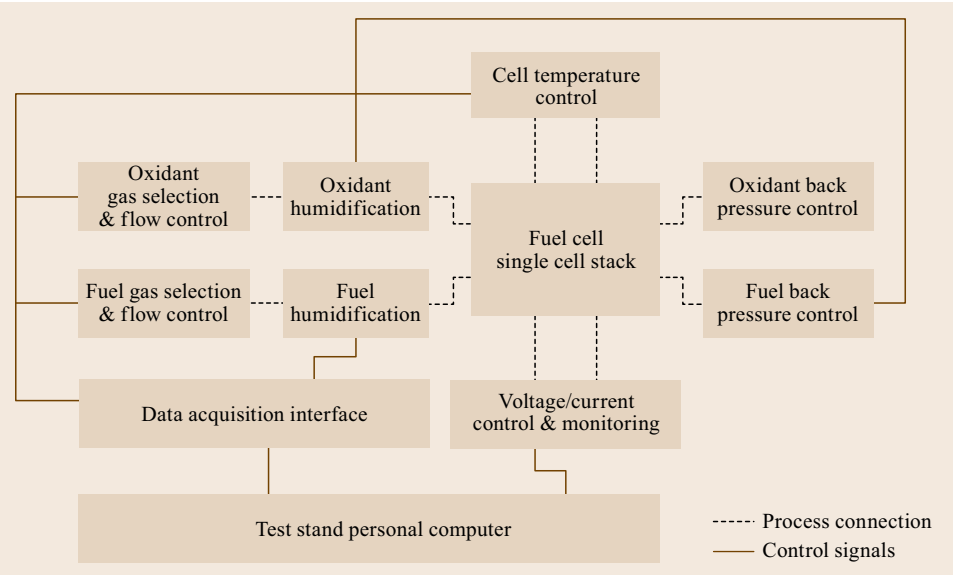

Fig. 19.4 Component subassemblies of a typical fuel cell test stand

cooling rates required, accuracy and stability and the flow range required. For example, for fuel cell tests with water-soluble contaminants, bubbler humidifiers are not acceptable whereas flash vaporization techniques are more suitable. Most test stations also include a dry bypass valve and circuit to provide dry purge gas for safety reasons (shutdown, freezing) or for more complex experiments such as those requiring fast relative humidity cycling.

Back Pressure Control. Thermodynamic, kinetic and mass transfer contributions to the PEMFC performance are affected by the reactant stream pressure [19.53]. The net effect is an increase in performance with pressure [19.54]. As a result, PEMFC operation requires a stable reactant stream pressure. This is accomplished by installing either a back pressure control valve or back pressure regulator on the fuel cell reactant stream outlets. Basic test systems are equipped with a pressure gage and a manual, spring loaded back pressure regulator installed downstream of the fuel cell. In this simple configuration, humidification and product liquid water, and reactant gases pass through the regulator causing instabilities. This system is improved by adding an outlet gas condenser to maintain a single phase gas stream passing through the regulator. Control flexibility is further improved by installing pressure transducers at the reactant inlets and outlets that provide feedback to the pressure control valve or regulator. Even greater flexibility is achieved by adding multiple pressure feedback points in the control software because testing protocol requirements vary (inlet versus outlet pressure control). The most stable systems utilize a dome loaded, back pressure regulator with a current-to-pressure converter controlling the dome pressure and operated by the controller feedback signal. Back pressure control valves are less stable. A back pressure regulator-based control system includes a set point/feedback control loop that interacts with the mechanical feedback loop located within the valve preventing pressure spikes during flow step changes.

Temperature Control. A PEMFC produces a relatively large amount of low-grade heat (50–70 °C) [19.55]. However, a single cell rapidly cools because the heat generated at the approximately two-dimensional thin catalyst layers (a few microns in thickness) is dissipated by contact with good heat conductors (carbon or metallic bipolar plates, metallic end plates). Therefore, the methodology used for cell temperature control depends on the cell or stack under test. Small-scale single cells, $< 50\,\mathrm{cm}^2$ in active area, utilize cartridge heaters installed in the end plates with cooling provided by natural convection. For larger cell sizes, forced cooling is required and is accomplished by attaching fans to the cell, either in a constant flow mode or controlled by the heater feedback controller cooling output. Surface heaters with custom shapes and providing a more uniform heating represent a convenient alternative to cartridge heaters. For specialized single cells and most small stacks, a coolant-based system is used, which also provides a subambient temperature option with the addition of a chiller and adequate cooling fluid [19.56]. A basic coolant system consists of a reservoir, heater, pump and rotameter for constant flow and temperature control. For stack testing,

increased complexity and flexibility are required including coolant flow and pressure, and temperature control. For example, stack testing may require a constant inlet temperature and pressure while maintaining a specific temperature gradient across the stack by varying the flow rate.

Voltage–Current Control. The normal fuel cell operating regime window extends from the open circuit potential to the limiting current ($\approx 0\,V$ or short circuit). A few situations exist that require fuel cell control within (existence of multiplesteady states [19.57, 58]) or outside (fuel starvation leading to cell reversal with a cell potential smaller than 0 V [19.59]) this operating regime window. Therefore, the fuel cell power output controlled by a load bank needs to be carefully assessed and selected from several possible modes: constant potential, current, power or resistance. Resistive load banks are commonly used but inductive load banks are available for more specialized test station needs. For single cells, a power supply may be used in series to boost the voltage level controlled by the load bank. The high current and low voltage output of the fuel cell is typically too low for most load banks. An integrated unit combining this power supply and load bank series arrangement is commercially available and marketed as a *zero volt* load bank. Bidirectional operational amplifiers or booster systems for potentiostats are also used in fuel cell test stands. Load banks are also equipped for the determination of the fuel cell ohmic resistance using current interrupt or frequency response analyzer-based techniques.

Data Acquisition and Hardware and Software Control. The data acquisition input and output hardware represents the test station core (Fig. 19.4). Most test stations include some form of signal conditioning and isolation, and acquisition hardware [19.60]. Information throughput is a function of the number and type of input-output channels, sample rate, and controller processor. Most test stations are also designed for static or quasistatic tests with time constants $\geq 10\,s$ and dwell times of several minutes. Dynamic tests require faster control and acquisition speeds with time constants in the range of milliseconds to seconds [19.48]. Recently, test stations have been designed with embedded controllers improving reliability and safety by reducing the intermediate role of a separate and remote computer working on a high-level operating system. Rather, safety features are integrated into the embedded controllers. Many test stations still rely on a computer for both software control and data visualization. The software provides control and execution of various experimental protocols as well as data storage and visualization. The more elaborate software packages provide flexible scripting features for automation, experiment control, test sequencing, and data processing and visualization.

Calibration

It is emphasized that each fuel cell test station control and measurement device needs to be calibrated. Mass flow controllers, pressure gages, thermocouples, relative humidity sensors and humidifiers, electronic load and data acquisition cards represent the most important elements to be calibrated. The overall test station performance also needs to be assessed with fuel cell tests to determine the synergy between the control and measurement devices.

A standard practice for calibration management involves the selection and identification of the systems and/or instruments requiring calibration, traceability requirements and a calibration frequency. A proper calibration program ensures system and equipment operational integrity and accuracy, and establishes measurements traceability to the United States National Institute of Standards and Technology (NIST) or other approved national measurement standards. Several documents provide guidance in this area (for example, United States Department of Defense standard MIL-STD-1839D). Calibration measurement tolerances and accuracies need to be established for specific equipment. Published standards provide guidance for the measurement uncertainty determination (NIST technical note 1297, American National Standards Institute [ANSI] NCSL Z540.2). At the organizational level, a quality control system for document management and supervision of calibration activities also needs to be established. Accreditation to an international quality standard such as ISO 17025 is not necessary, especially for academic institutions and national laboratories. The ISO 17025 standard is well beyond the level required to ensure the competence of a fuel cell testing laboratory and need to be viewed as a guideline. As a general rule of thumb, equipment calibrations need to be completed with a master meter that is more accurate than the device under test by a factor of ≈ 4 (United States Department of Defense standard MIL-STD-1839D). The master meter needs to be calibrated by an ISO 17025 accredited metrology laboratory, providing traceability to a national standard. The decision to acquire master meters depends on cost (cost and number of calibrations to be completed by an external certification laboratory, master meters cost and calibration cost) and convenience.

The combined system operation also needs to be validated using standardized procedures. The United States Department of Energy and members of the Fuel

Cell and Hydrogen Energy Association initiated programs to establish a standardized test procedure for single-cell PEMFCs. A round robin test series was conducted with several organizational participants with the objective to verify the validity of the proposed standardized test protocols (United States Fuel Cell Council documents 04-011B and 05-014B.2). The European Commission supported similar efforts to address the aspects of prenormative research, benchmarking, and validation through round robin testing under the Fuel Cell Systems Testing, Safety, and Quality Assurance program.

19.3 Fuel Cell Stack Components and Assembly

Fuel cell stack design depends on the application [19.61]. For instance, automotive design is largely dictated by power density whereas stationary design requires durability. For portable applications, design criteria as well as manufacturing methods are much more varied. This is due in part to the restricted space and resulting trend towards a planar stack design that simplifies the compression mechanism and enables the use of manufacturing methods for thin, multiple layers. For each application, it is desirable to avoid the introduction of undesirable species during stack manufacturing and assembly. The assembly of all stack components in the proper sequence is also important to ensure integrity and avoid leaks to the ambient air or from one compartment to another. Therefore, the stack assembly and its interface to the test station or balance of plant need to be verified.

19.3.1 Hardware Design and Manufacturing

A commonly used single fuel cell assembly is discussed as an illustrative and widely representative example. Most fuel cell data are obtained with a single fuel cell. Single cells range from small scale (material evaluation) to full scale size for component evaluation (manifold, flow field, seal, MEA, etc.). For a stack, the assembly procedure is relatively similar with several steps being repeated to achieve the desired number of cells.

An assembled single-cell PEMFC is depicted in Fig. 19.5a and the visible hardware components are identified. A more detailed list of all components and their functions is given in Table 19.4 and discussed in [19.61]. Cited references contain materials used for component production and in several cases methods for performance optimization and durability considerations. A detailed design and manufacturing process review including material selection was also prepared for several PEMFC hardware components [19.62].

An expanded view of the single-cell hardware is given in Fig. 19.5b. Major components are shown with the exception of the gas diffusion media and the MEA, which are located between gas flow field plates. The MEA consists of the anode and cathode catalyst and catalyst support material deposited onto the proton conductive membrane (the catalyst coated membrane or CCM) and the gas diffusion media. If the catalyst layer is deposited onto the gas diffusion medium, the resulting component is referred to as a gas diffusion electrode (GDE). Stacks consist of several single cells with gas flow field bipolar plates that are electrically connected in series to enable higher output voltages. A PEMFC stack design is illustrated in Fig. 19.6 [19.62].

19.3.2 Cell and Stack Components Cleaning

The use of laboratory gloves made of the appropriate material is imperative whenever handling fuel cell components during assembly and cleaning. Gloves provide protection from chemical cleaning agents and avoid contamination of fuel cell components from skin oils. Newly machined fuel cell components need to be cleaned to remove dirt, oil and other residues from the fabrication process. For example, silicon from the gasket migrated to the catalyst layer and membrane and was deemed partly responsible for the observed degradation [19.67]. Additionally, subsequent to fuel cell testing, the test station components may need to be cleaned to remove any residual contaminant that was purposefully added. A number of cleaning strategies and agents are available including from component suppliers.

Fuel cell hardware components are typically removed from the test station and disassembled before cleaning is accomplished using an ultrasonic bath. Cleaning agents are listed in Table 19.5. In general, the use of organic solvents as cleaning agents is limited due to their detrimental effect on cell performance [19.35]. Care should be exercised to avoid damage caused by the ultrasonic bath to sensitive hardware components. For example, the treatment of graphite materials or materials coated with thin anticorrosive layers should be avoided. For these specific cases, alternative cleaning methodologies are necessary such as rinsing with extended durations and compatible cleaning agents.

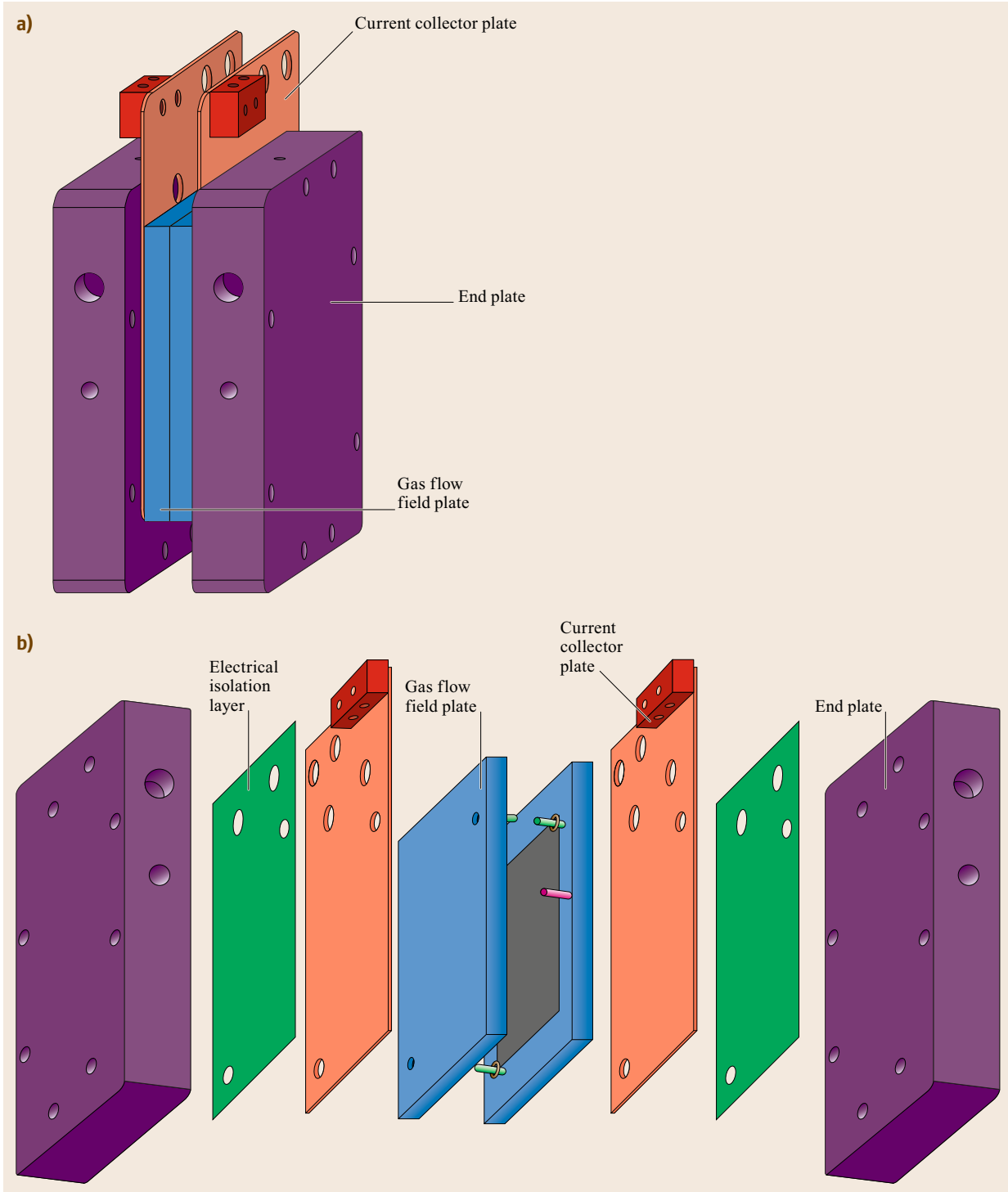

Fig. 19.5a,b PEMFC assembled in a single cell configuration (a). PEMFC expanded view (b). Tie bolts are not displayed for simplicity

Table 19.4 Fuel cell hardware components and functions

Hardware component	Function	References
End plate	Provides compressive force which seals the cell from leaks and minimizes the electrical resistance of the hardware components	*St-Pierre* [19.61]
Bipolar gas flow field plate	Electrically conductive material with channels that enable the gas to flow through the cell	*Mehta* and *Cooper* [19.62], *Tawfik* et al. [19.63]
Seal	Material used to prevent overboard gas leakage	*St-Pierre* [19.61]
Gas diffusion media	Porous media, which is often carbon based, that is placed adjacent to the membrane/electrode assembly to facilitate the transport of gases and water in liquid and vapor phase	*Mehta* and *Cooper* [19.62], *Nam* and *Kaviany* [19.64], *Lin* and *Van Nguyen* [19.65]
Cooling plate	Used for temperature regulation of the fuel cell	*St-Pierre* [19.61, 66]
Membrane–electrode assembly	Consists of anode and cathode electrode catalyst layers deposited onto a proton conductive membrane	*St-Pierre* [19.61], *Mehta* and *Cooper* [19.62]

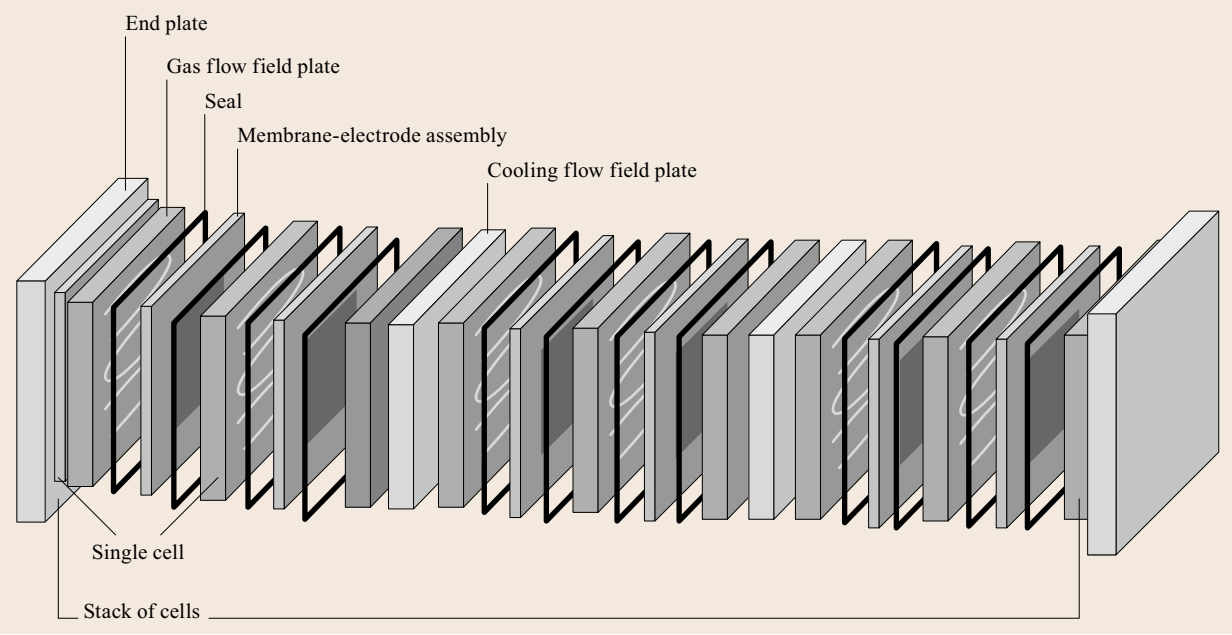

Fig. 19.6 PEMFC stack hardware components. Flow field channels are formed on a bipolar plate noted here as a gas flow field plate (after [19.62])

Table 19.5 Cleaning agents for fuel cell hardware components

Cleaning agent	Examples	Usage precautions	Ultrasonic bath compatibility
Deionized water	–	Can be corrosive to metals	Yes
Organic solvents	Isopropanol, methanol, ethanol, acetone	Possible detrimental effects of solvent residue on PEMFC performance	No
Detergents	Alconox, Liquinox	Materials may be incompatible	Yes
Acidic cleaners	Citranox	Materials may be incompatible	Yes

19.3.3 Single Cell Assembly

The assembly of a single fuel cell with component designs that are commonly used in many fuel cell testing laboratories is discussed as an illustrative example of the design-dependent assembly of a single fuel cell or stack. Commercial fuel cell designs have additional design features that minimize or avoid assembly errors. A successful assembly is achieved with proper component alignment and adequate mechanical compression to mitigate electrical efficiency losses due to contact resistances between components, gas and

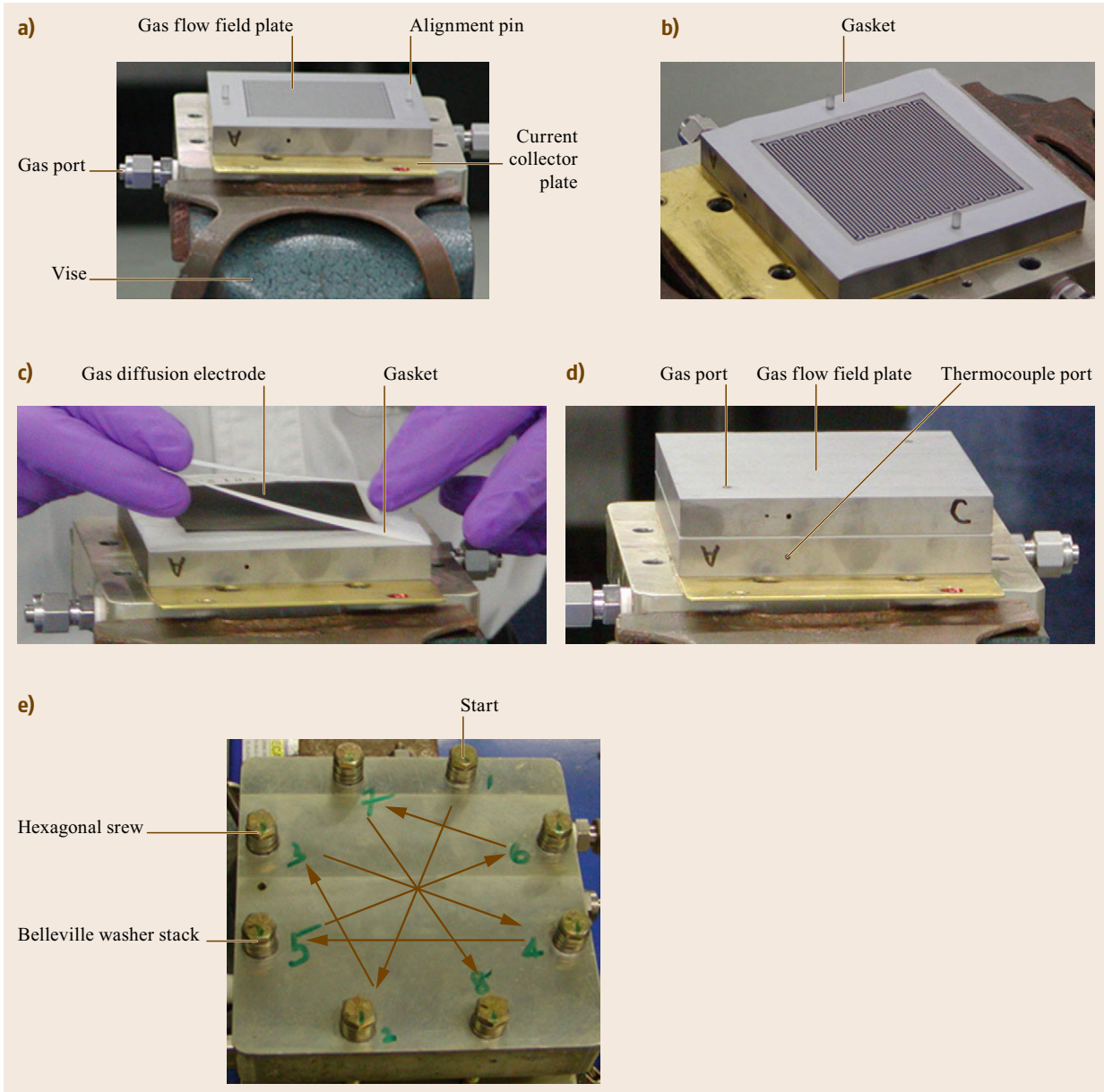

Fig. 19.7a–e Anode end plate, electrical insulation layer, current collector and gas flow field plate **(a)**, gasket seal attached to the anode gas flow field plate **(b)**, MEA and second gasket seal attached to the anode compartment parts **(c)**, cathode gas flow field plate attached to the cell assembly **(d)**, hexagonal head screws sequential tightening scheme to optimize compression across hardware components **(e)**

coolant leakages and to optimize reactant transport and water management within the GDE by avoiding reactant flows bypass and structural collapse of the porous components. This is achieved by selecting the appropriate gasket thickness to match a specific gas diffusion layer (GDL).

Figure 19.7a shows the anode end plate, electrical current collector and anode gas flow field plate during assembly. The gas flow field plate has holes for the attachment of alignment pins which serve to align the anode and cathode flow field plates in addition to the gasket seals and MEA. The end plates are made

of aluminum, the current collector plates of gold-plated copper to minimize the contact resistance and the flow field plates of electrically conductive POCO graphite. The current collector plate is electrically isolated from the end plate by an insulating layer of polymer which is typically polytetrafluoroethylene. The hardware components are assembled by stacking them together so that the inlet and outlet holes on the gas flow field plates align with their counterpart holes on the end plate.

Once the hardware components of the anode side are properly aligned, the first of two gasket seals is applied to the cell. The gasket alignment is maintained by two alignment pins as shown in Fig. 19.7b. After the first gasket is in place, the MEA, which in this case consists of the CCM and a porous carbon layer on both the anode and cathode, is placed onto the assembly while the alignment is still maintained by the pins (Fig. 19.7c). The cathode flow field plate is added to the assembly as demonstrated by Fig. 19.7d. The alignment pins shown in Fig. 19.7a,b serve to maintain the correct placement of the flow field plate. Finally, all fuel cell elements are secured together with screws (Fig. 19.7e). Belleville washers are also added to ensure that compression is maintained at a relatively constant level even if the membrane absorbs water or dehydrates, affecting its thickness [19.68]. Other compression mechanisms are equally adequate [19.61]. The cell assembly proceeds using a calibrated torque wrench with one quarter turns to the hexagonal head screws in a cross tightening pattern until the necessary torque is obtained (Fig. 19.7e).

19.3.4 Cell Assembly Verification

Gas leak rates are determined by using a fixed volume vessel containing nitrogen (or a different inert gas such as helium), pressurized to approximately 5 bar and alternatively connected to the fuel cell anode and cathode inlet reactant gas lines. The 5 bar pressure is suitable for an ambient pressure fuel cell operation, otherwise, for higher pressures, it needs to be adapted. The fuel cell pressure is maintained at approximately 2 bar by a pressure regulator. The 1 l vessel change in pressure is measured over time to calculate the gas leakage rate. The acceptable leakage rate is determined by the cell or stack manufacturer specifications because it is design dependent. A leak is located by submerging a pressurized cell or stack into a deionized water bath. The cell or stack may be subsequently disassembled to determine the cause of the leak and develop preventive measures. If the fuel cell or stack has a coolant circuit, it also needs to be verified for leakage using the same pressurized gas approach. Other leak detection methods exist. For instance, a compartment is pressurized and subsequently isolated with a valve. The subsequent decrease in pressure is monitored and the rate of change indicates the leak size.

Adequate component compression is required to minimize electrical resistance and optimize the GDE performance [19.61, 69]. The optimal compression is dictated by the stack design, component materials and reactant stream pressures. The compression is evaluated by modifying the cell assembly procedure with a pressure-sensitive paper inserted between a flow field plate and the MEA. Subsequently, the cell is dismantled and the pressure-sensitive paper is retrieved for analysis. The resulting color change intensity and distribution is used to estimate the compression magnitude and uniformity across the cell active area.

Electrical short circuits are not desirable because they affect the cell performance evaluation. The presence of an electrical short circuit between the current collector plates and the end plates is easily assessed by measuring the resistance with a multimeter. The presence of a short circuit through the MEA is design dependent and is important to also assess. For flush cut MEA designs where the catalyst and GDLs extend to the membrane edge [19.61], there is a possibility that the thin membrane thickness is bridged by longer GDL carbon fibers. For this specific case, dry inert gases are circulated through the assembled cell and a power supply is used to apply a voltage lower than ≈ 1 V to avoid any electrochemical reactions (water electrolyzer and fuel cell modes) and focus on the electronic conductivity. A multimeter is also used to measure the resulting current allowing the calculation of the electrical resistance. If short circuits are detected, the cell is disassembled to find the cause and devise preventive measures.

19.3.5 Installation into the Test Station

After the cell or stack assembly has been verified, the unit is interfaced with the test station. This step requires the completion of several connections to the reactant gas supplies, coolant supply, load bank and sensors. It is assumed that the test station operation has also been verified especially for fluids leakage using similar methods as described in Sects. 19.2.2 and 19.3.4. Subsequently, the unit is conditioned and tested using methods that are respectively described in Sects. 19.4.1 and 19.4.2.

19.4 Testing and Diagnostic Techniques

The research focus is dependent on many factors that include organization type (academic institutions, national laboratories, companies), resource availability (human, equipment, funds), mission and needs as defined by customers [19.70]. In turn, the research focus defines the selection of testing and diagnostic techniques. These considerations lead to multiple options and underline the variability in research capabilities at fuel cell active institutions.

The HiSERF scope is schematically depicted in Fig. 19.8 and includes fuel cell activities ranging from material, single cell and stack characterization to system level evaluations. Such a wide scope was deemed advantageous and necessary to adapt to customer demands but also to ensure that all different levels effects of interest can be studied and interrelated. For example, a catalyst tested with a rotating ring-disc electrode dipped into a liquid aqueous electrolyte is not representative of the single fuel cell environment with a solid electrolyte. Single cells in a fuel cell stack do not necessarily behave in a similar manner as local operating conditions vary (reactant distribution is not uniform, end cells are cooler in proximity to the heat conductive end plates, etc.). A fuel cell stack is also subjected to different operating conditions in a test station and an application because respective components have different transient response times and operating ranges.

For each activities scope shown in Fig. 19.8, many test options are available and include ex situ tests to generally obtain material related information, and in situ tests with either modified or nonoperating conditions to characterize the fuel cell performance and predict behavior in an application or extract specific parameters to clarify fundamental understanding. A clear purpose needs to be established considering the number of test choices available. From that standpoint, it is useful to consider the different processes taking place in a fuel cell (Fig. 19.9). Mass and heat transfer, charge transfer, reaction kinetics, degradation and other processes take place over a wide range of time scales that do not necessarily overlap thus offering opportunities to focus on specific aspects by tailoring tests. For example, degradation due to contaminants is easily separated from liquid water processes using in situ life tests. However, precautions are still necessary to minimize other degradation mechanisms such as catalyst dissolution and agglomeration. This is achieved with accelerated tests and higher contaminant concentrations, and by maintaining the cell and cathode potential below the Pt oxidation potential. Other test selection considerations include cell voltage loss types, envisaged applications and the existence of standardized protocols with the recognition that many other options exist. For instance, an ex situ membrane conductivity cell is appropriate to understand the effect of gaseous or liquid contaminants on cell voltage ohmic losses. Steady-state performance tests are preferable over hardware in the loop transient tests for stationary applications as the load is expected to slowly vary.

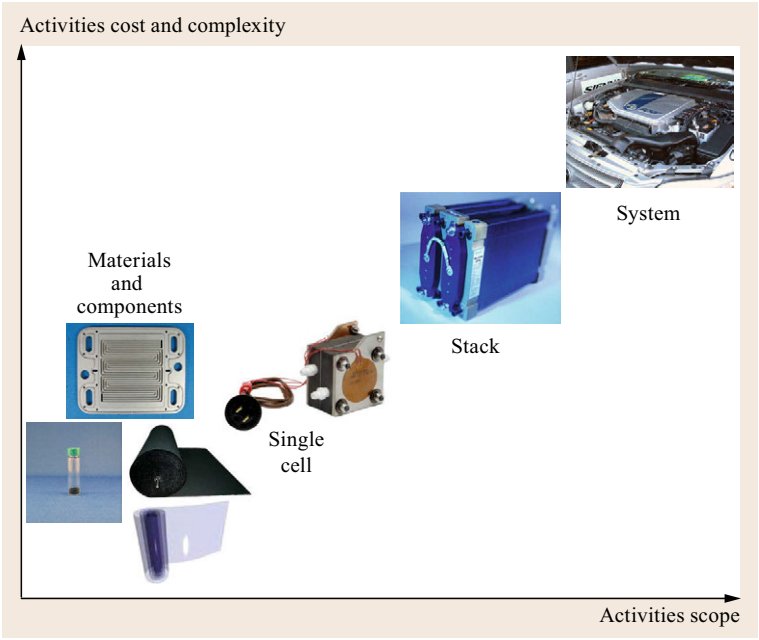

Fig. 19.8 HiSERF PEMFC activities scope

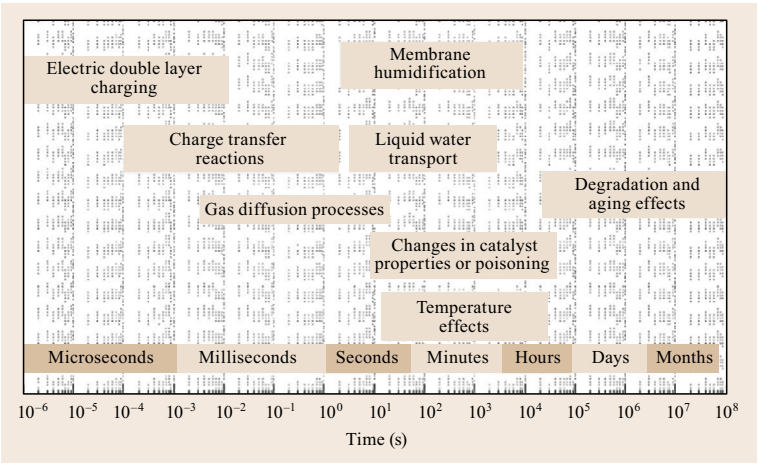

Fig. 19.9 PEMFC processes relaxation time scales

Rather than selecting tests and diagnostic techniques to meet a particular goal, there is also value in assessing gaps. For instance, a large number of techniques have been developed to characterize fuel cell performance. Ten techniques were reviewed for the sole purpose of quantifying the presence of liquid water [19.11]. A detailed review of all techniques irrespective of their purpose is outside the scope of the present chapter. Rather, suggestions for high level analyses are presented to facilitate the identification of gaps in measurement techniques. As a first example, the fuel cell is analyzed at a high level in terms of the fuel cell inputs and outputs: reactants provided and products, power and heat generated (Fig. 19.2). Each technique was classified in these categories using its main objective. Results from this analysis using common and representative techniques without being exhaustive are listed in Table 19.6. Several well-established methods are available to characterize the fuel cell performance, the quantity and nature of the products (main and resulting from side reactions or degradation mechanisms), and reactants (main and present due to imperfections in purification processes). However, few correlations have been established between the different methods especially to take advantage of the potential synergy associated with complementary temporal or geometric resolution. Furthermore, few techniques with sufficient resolution are available to characterize heat transfer (a few ex situ techniques were also presented [19.71–73]). This statement applies to both fuel cell and other operation modes. Thermocouples are approximately of the same dimensions as the thin MEA components (tens to hundreds of microns) creating an accuracy issue. An infrared camera only provides the cell outside temperature. Improved techniques are needed because water management including temperature-driven water transport [19.74] is very sensitive to temperature gradients corresponding to a temperature change of less than a degree Celsius [19.75]. In addition, it was proposed that heat is generated at the cathode whereas heat is consumed at the anode [19.55]. This hypothesis has not yet been experimentally verified. Difficulties associated with the steep temperature gradient measurement is likely responsible for the relatively more numerous modeling activities [19.76]. Supplementary references to Table 19.6 are provided and discussed in Sect. 19.4.2.

Other high level analyses are possible by focusing on other aspects. As a second example, an analysis performed by targeting geometric resolution has revealed that few techniques exist to characterize fuel cells in the cross-channel or through-plane direction [19.98]. Furthermore, many of these geometrically sensitive methods, including those resolving the channel length direction, appear to be seldom used. Another gap exists in relation to methods specifically developed to explore the behavior of stacks, or in other words cell to cell variability, especially in the presence of faults [19.76, 99–101]. Other approaches are possible to identify test and diagnostic technique gaps by focusing on other relevant aspects such as component manufacturing quality control.

In the next section, general test considerations are highlighted. In the subsequent two sections, a few widely applied in situ and ex situ tests are described whereas other more specialized tests are discussed at the high level as detailed descriptions are deemed outside the scope of this chapter.

19.4.1 Conditioning

After the PEMFC is assembled, a conditioning or break-in period is needed to activate and increase catalyst utilization by accessing the catalyst layer inactive regions. This activation normally requires ionomer

Table 19.6 Diagnostic techniques using a PEMFC in different operating modes

Operating mode	Method	Method focus	Reference
Fuel cell	Polarization curve	Electrical power output	*Reshetenko* et al. [19.30]
	Segmented cell	Electrical power output	*Reshetenko* et al. [19.30]
	Impedance spectroscopy	Electrical power output	*Barsoukov* and *MacDonald* [19.77], *Orazem* and *Tribollet* [19.78]
	Current interrupt	Electrical power output	*Büchi* et al. [19.79]
	Residence time distribution	Products	*Diep* et al. [19.38], *St-Pierre* et al. [19.39]
	Neutron imaging	Products	*Mukundan* and *Borup* [19.80]
	X-ray diffraction	Products	*Isopo* et al. [19.81]
	Transparent cell	Products	*Tüber* et al. [19.82], *Yang* et al. [19.83]
	Water collection and analysis	Products	*Young* et al. [19.84]
	Gas chromatography, mass spectroscopy	Reactants, products	*Bender* et al. [19.85], *Schuler* et al. [19.86]
	Thermocouples	Heat	*Vie* and *Kjelstrup* [19.87]
	Infrared camera	Heat	*Matian* et al. [19.88]
Other	Electronic short circuit	Electrical power output	*Kocha* et al. [19.89]
	Cyclic voltammetry	Electrical power output	*Vielstich* [19.90], *Lindström* et al. [19.91]
	Linear sweep voltammetry	Reactants	*Kocha* et al. [19.89], *Inaba* et al. [19.92]
	Segmented cell with different gas diluents	Reactants	*Reshetenko* and *St-Pierre* [19.93]
	Membrane permeability	Reactants	*Kocha* et al. [19.89], *Broka* and *Ekdunge* [19.94]
	Electroosmotic drag	Products	*Choi* et al. [19.95], *Peng* et al. [19.96]
	Water collection and analysis with inlet contaminants	Reactants, products	*Wetton* and *St-Pierre* [19.97]

and membrane humidification. Several reasons explain this situation because reactants reach the catalyst sites but protons cannot, some ionomer sites are less easily hydrated (the ionomer structure is not isotropic) and electrons cannot reach the catalyst sites (partial electronic phase continuity) [19.102, 103]. After conditioning, the fuel cell achieves peak performance with a constant current at a specific voltage that is desirable for research purposes. Rapid and reproducible conditioning methods have been developed by different fuel cell organizations or research institutes (Table 19.7). For instance, the use of a hydrogen pump mode (United States Fuel Cell Council Document 04-003) and CO stripping [19.104] have also been proposed. The conditioning procedure is interrupted after the cell performance for both rated and quarter power reaches a value that is within 2% of the manufacturer's specification or expected value (United States Fuel Cell Council document 04-003).

19.4.2 In Situ Tests

Several categories of in situ tests are distinguished by their objectives. The fuel cell performance is of immediate commercial value as operating conditions change during fuel cell use. As a result, steady-state tests of different duration (short or long term) as well as transient tests including duty cycling are relevant. Hardware in the loop tests aiming at the interactions between fuel cell system balance of plant components and the fuel cell stack are also of interest (Fig. 19.3). Diagnostics are also needed to unravel mechanisms and facilitate the development of improved and more durable fuel cells. Test results are equally needed to validate mathematical models used to predict fuel cell performance and extract model parameters. All three categories are further discussed in the next section. In subsequent sections, the emphasis is given to the use of electrochemical characterization techniques whereas others are only briefly discussed.

Test Types

The performance of PEMFCs is characterized either under constant or varying power conditions. For constant power, the current density of a cell or stack is typically fixed and the resulting voltage is measured. For single cells, a constant potential is easily applied but is problematic for a stack as control is more difficult.

Table 19.7 Standardized conditioning procedures summary

Organization	Operating conditions	First stage	Second stage	Third stage
FCHEA (USA)	80 °C cell temperature H_2/air 1.7/1.7 barg pressure 100/100% relative humidity 1.2/1.5 stoichiometry	Decrease cell voltage until 600 mV is reached and maintain for 1 h	Cycle cell voltage for 6 h between 0.5/0.7 V with a 20 min dwell time	Maintain 0.2 A/cm^2 during 18 h
DOE (USA)	80 °C cell temperature H_2/air, N_2, or O_2 atmospheric pressure 100/75% relative humidity 3/3.6 stoichiometry	Circulate saturated H_2/N_2 on anode/cathode for 3 h	Maintain cell voltage at 0.55 V with H_2/air	Sweep out to the limiting or maximum current density with H_2/air, H_2/O_2
FCTESTNET (European Union)	80 °C cell temperature H_2/O_2 3/3 barg pressure 100/100% relative humidity 1.2/1.5 stoichiometry	Increase current until 1 A/cm^2 is reached and keep cell voltage > 500 mV	Maintain 1 A/cm^2 during 18 h	–
JARI (Japan)	Maintain 0.2 A/cm^2 during 18 h 80 °C cell temperature H_2 or N_2/air or N_2 atmospheric pressure 100/100% relative humidity 1.4/5.5 stoichiometry	Circulate dry N_2/N_2 for 1 min and 22 s at 200/200 ml/min before the cell is heated	Increase current density to 1 A/cm^2 and maintain until cell voltage is stable	–

United States Fuel Cell Council document, 05-014B.2, (after [19.8, 9, 105–107])

Operating parameters such as the reactant gas flow stoichiometries, reactant pressures, cell temperature, and inlet stream relative humidity are held constant. For dynamic measurements, the load across the cell or stack is varied and the corresponding change in voltage is measured. During dynamic measurements, the cell operating parameters change as a result of the changing power output unless the fuel cell test station or system is designed for a rapid response and constant operating conditions.

There are several documents that discuss methods to measure performance. For example, an experimental setup that enables excellent stability of system operating parameters for steady-state performance measurements was described [19.85]. A method for extrapolating performance loss during steady-state operating conditions from a limited amount of performance data was provided [19.108]. Steady-state tests also extend to long durations to establish durability. Such tests typically run from 1000 to 10 000 or more hours [19.109–113]. Such tests are useful but do not necessarily reproduce the observed behavior in the field as operating conditions are not constant. As a result, tests are increasingly completed under dynamic conditions simulating drive or duty cycles in applications [19.114–117]. Furthermore, long-duration tests consume significant resources (low turnover). This additional pressure has led to the development of a number of accelerated tests targeted at specific degradation mechanisms. A consistent set of accelerated protocols is available from the United States Department of Energy for known degradation mechanisms involving key MEA materials: electrocatalyst, catalyst support, and membrane (Table 19.8). An overview of the durability test protocols that were developed through 2011 is available [19.118]. Additional work discussing accelerated testing methods recently appeared [19.119, 120].

A fuel cell requires support components to operate (Fig. 19.3). On the other hand, a fuel cell test station does not mimic the fuel cell system balance of plant behavior. Therefore, it is important to test the fuel cell under system compatible operating conditions. This is achieved with the use of hardware in the loop technique. This concept is illustrated in Fig. 19.10. A fuel cell and optionally a few balance of plant components are integrated into a fast dynamic response test station that is controlled using a model of the remaining balance of plant components [19.48, 49, 121]. In effect, the behavior of the balance of plant is simulated in real time with a combination of a balance of plant components model and the fast response test station. The hardware in the loop technique is useful to evaluate the fuel cell dynamic response under practical, steady-state or long-term operating conditions, control algorithms and controllers, and new system layouts or components. The test station dynamic response needs to be smaller than 100 ms to ensure that the fastest system component is simulated in real time.

Table 19.8 United States Department of Energy accelerated material and component durability tests

Test parameters	Test objective			
	Electrocatalyst	**Catalyst support**	**Membrane/electrode assembly chemical stability**	**Membrane mechanical stability**
Cycle	50 mV/s between 0.6 and 1.0 V, triangular sweep cycle, 25–50 cm^2 single cell	Hold at 1.2 V for 24 h, run polarization curve and electrochemical surface area, repeat for a total of 400 h, 25–50 cm^2 single cell	–	Cycle from 0% relative humidity (2 min) to 90 °C dew point (2 min), 25–50 cm^2 single cell
Number (cycle)	30 000	–	–	–
Cycle time (s)	16	–	–	–
Temperature (°C)	80	80	90	80
Relative humidity (%)	Anode-cathode, 100/100	Anode-cathode, 100/100	Anode-cathode, 30/30	Cycle from 0% relative humidity (2 min) to 90 °C dew point (2 min)
Fuel/oxidant	Hydrogen-N_2 (H_2 at 200 standard cm^3/min and N_2 at 75 standard cm^3/min for a 50 cm^2 cell)	Hydrogen-N_2	Hydrogen-air, 0.2 A/cm^2 and 10/10 stoichiometry equivalent flow	Air-air, 2/2 standard l/min
Pressure (kPa absolute)	0	150	150	0
Total time (h)	–	400 (continuous operation)	500	Until crossover > 2 mA/cm^2 or 20 000 cycles
Diagnostic frequency (h)	–	24	–	–
Test condition	–	–	Steady-state open circuit potential, 25–50 cm^2 single cell	–
Catalytic mass activity[a]	At beginning and end of test (minimum), ≤ 40% loss of initial catalytic activity	Every 24 h, ≤ 40% loss of initial catalytic activity	–	–
Polarization curve[b] from 0 to ≥ 1.5 A/cm^2	After 0, 1 k, 5 k, 10 k and 30 k cycles, ≤ 30 mV loss at 0.8 A/cm^2	Every 24 h, ≤ 30 mV loss at 1.5 A/cm^2 or rated power	–	–
Electrochemical surface area/cyclic voltammetry[c]	After 10, 100, 1 k, 3 k, 10 k, 20 k and 30 k cycles, ≤ 40% loss of initial area	Every 24 h, ≤ 40% loss of initial area	–	–
F^- release or equivalent for non-fluorine membranes	–	–	At least every 24 h, no target (for monitoring purposes)	–
Hydrogen crossover[d]	–	–	Every 24 h, ≤ 2 mA/cm^2	Every 24 h, ≤ 2 mA/cm^2
Open circuit potential	–	–	Continuous, ≤ 20% loss in OCV	–
High frequency resistance	–	–	Every 24 h at 0.2 A/cm^2, no target (for monitoring purposes)	–
Shorting resistance[e]	–	–	Every 24 h, > 1000 Ωcm^2	Every 24 h, > 1000 Ωcm^2

[a] Mass activity in A/mg at 150 kPa absolute back pressure and 857 mV (ohmic loss corrected) on 6 % H_2 (balance N_2)-O_2 (or equivalent thermodynamic potential), 100% relative humidity, 80 °C, normalized to initial mass of catalyst and measured before and after test
[b] Recommended polarization curve protocol
[c] Sweep from 0.05 to 0.6 V at 20 mV/s, 80 °C, 100% relative humidity
[d] Crossover current as described in United States Fuel Cell Council document 05-014B.2, section A3-2
[e] Measured at 0.5 V applied potential with N_2-N_2, 80 °C and 100% relative humidity. Compression to 20% strain on the gas diffusion layer

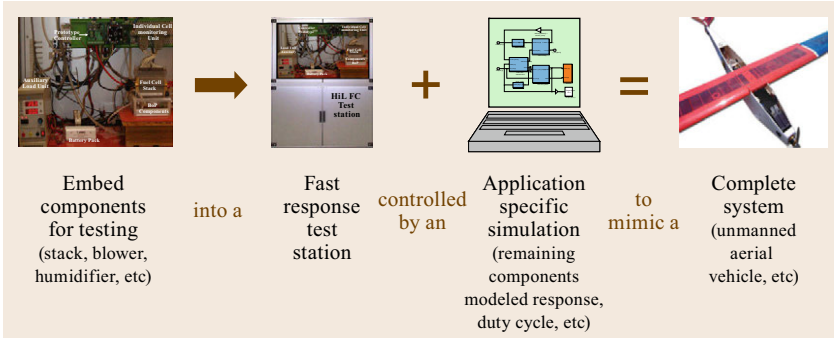

Fig. 19.10 Hardware in the loop operational concept

Diagnostics are added to the main purpose fuel cell performance test to supplement fuel cell characterization data or facilitate interpretation. The selection of the most appropriate diagnostics is crucial to balance time and resources, and information needs. Furthermore, the diagnostics selection may affect the outcome of the main test by introducing artifacts. For example, long term fuel cell tests are relevant to establish the durability of Pt alloy catalysts. However, the measurement of the cell current density or voltage does not yield the evolution of the key metric, the catalyst surface area. A more direct method is needed. Cyclic voltammetry has been used to intermittently evaluate the surface area of Pt catalysts with information obtained in the hydrogen adsorption, hydrogen desorption or CO adsorption regions (voltammetry Sect. 19.4.2). For Pt alloy catalysts, cyclic voltammetry does not lead to the desired active area value because the alloying element either dissolve at a specific potential thus accelerating catalyst degradation or the method is unreliable because the probe molecule adsorption is different on the alloy than on Pt [19.122].

Finally, there are a number of tests typically performed to evaluate MEA properties in situ for modeling validation or diagnostic purposes. For example, a polarization curve is able to provide cathode catalyst kinetic parameters as long as the low current density region is investigated (Tafel behavior) and the membrane crossover H_2 flux is measured for current density correction [19.123]. However, the membrane crossover H_2 flux requires a specific test [19.106]. Other parameters of interest include transport properties (mass and heat) in the gas and solid phases (ionomer/membrane, electrodes, bipolar plates), and main and side reaction rate constants.

Polarization

The H_2–air performance curve, also known as the polarization curve or the current density-voltage ($I-V$) curve, represents the baseline PEMFC performance diagnostic. A polarization curve (Fig. 19.11) generally shows

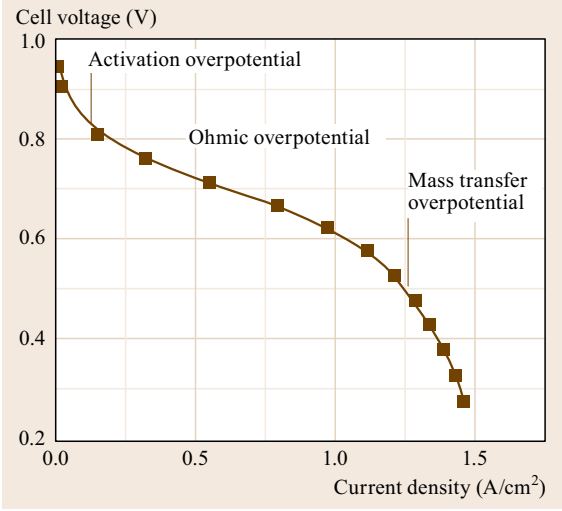

Fig. 19.11 PEMFC polarization curve with three distinct regions

three distinct regions at different current densities, that each indicate the predominance of one process, activation, charge transfer or mass transfer [19.124–126]. Activation losses are associated with slow oxygen reduction kinetics, which are described by the Butler–Volmer equation (19.1). The current density j (A/cm^2) is a function of the exchange current density j_0 (A/cm^2), the electron transfer coefficient α, the number of exchanged electrons n, the Faraday constant F (96 500 C/mol), the activation polarization η_{act} (V), the gas constant R (8.31 J/mol K) and the temperature T (K):

$$j = j_0 \left[\exp\left(\frac{\alpha n F \eta_{act}}{RT}\right) - \exp\left(-\frac{(1-\alpha) n F \eta_{act}}{RT}\right)\right]. \quad (19.1)$$

For large reduction currents leading to an activation polarization that exceeds the limit given by (19.2), the reverse reaction is negligible and (19.1) reduces to the

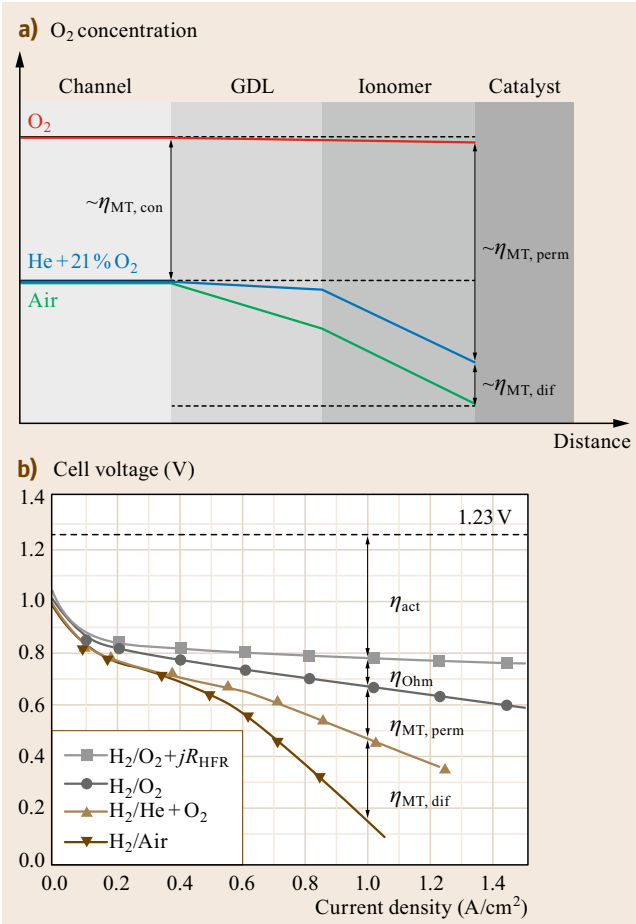

Fig. 19.12a,b O_2 concentration profiles in a PEMFC for different cathode gas supply: O_2, He + O_2, air **(a)**. Polarization curves obtained with H_2-O_2, H_2/He + O_2, H_2-air **(b)**. Anode-cathode conditions: 2/2 stoichiometry, 100/50% relative humidity, 48.3/48.3 kPag, 60 °C

Tafel equation (19.3)

$$|\eta_{act}| \gg \frac{RT}{nF} = \frac{25.7}{n}\text{mV} \quad (\text{at } 25\,^\circ\text{C})\,, \tag{19.2}$$

$$\eta_{act} = \frac{RT}{\alpha nF}\ln j_0 - \frac{RT}{\alpha nF}\ln j\,. \tag{19.3}$$

Ohmic losses η_{Ohm} (V) occur due to limitations associated with protonic and/or electronic charge transport, which linearly increase with the cell current density (Ohm's law, (19.4)). The high frequency resistance denoted by R_{HFR} (or serial resistance, Ωcm^2), is divided into a protonic membrane resistance (R_m, Ωcm^2) and an electronic resistance for electrodes and other electric circuit elements (R_e, Ωcm^2). The high frequency resistance of a fuel cell R_{HFR} is determined during fuel cell operation using electrochemical impedance spectroscopy (EIS):

$$\eta_{Ohm} = R_{HFR}j = (R_m + R_e)j\,. \tag{19.4}$$

The local consumption of O_2 in air, a gas diluted with 79% N_2, creates a local depletion at the catalyst surface and mass transfer losses. Mass transfer losses are described by (19.5) [19.127], which indicates that polarization losses significantly increase when the catalyst surface reactant concentration approaches zero at high current densities j near the limiting value j_l (A/cm^2):

$$\eta_{MT} = -\frac{RT}{nF}\ln\left(1 - \frac{j}{j_l}\right) \tag{19.5}$$

Mass transfer losses are further decomposed into permeability and diffusion components [19.30, 128]. Figure 19.12a illustrates O_2 concentration profiles for different gas compositions. The O_2 concentration is approximately constant from the gas channel to the catalyst surface because only a relatively small amount of water vapor is present in the gas stream. The O_2 polarization curve constant slope at high current densities (ohmic behavior, absence of significant mass transfer losses, Fig. 19.12b) is an alternative to the R_{HFR} measurement with EIS. For a 79% He + 21% O_2 mixture, the O_2 concentration is lower with a small decrease in O_2 concentration in the gas phase, which is limited by the high value of the oxygen diffusion coefficient in He. The decrease in O_2 concentration is more significant in the ionomer phase. For the air case, the O_2 concentration gradient is more significant in the gas phase because the O_2 diffusion coefficient is smaller with a heavier N_2 diluent than with He (diffusion coefficients of an equimolar mixture of O_2–He and O_2–N_2 are 0.723 and 0.202 cm^2/s at 293 K and 101.325 kPa [19.129]). In the ionomer phase, the O_2 concentration profiles for air and the He + O_2 mixture lead to a similar concentration difference (Fick's first law with the same diffusion coefficient and diffusion length). The difference between O_2 and the He + O_2 mixture polarization data defines the permeability overpotential $\eta_{MT,perm}$ (the largest concentration difference is located in the permeable ionomer). The difference between the He + O_2 mixture and air polarization data defines the diffusion overpotential $\eta_{MT,dif}$ (corresponds to the approximate concentration difference in the porous GDE with predominant diffusive transport). The sum of $\eta_{MT,perm}$ and $\eta_{MT,dif}$ corresponds to η_{MT} (19.5).

Figure 19.12b shows polarization curves measured for the three cathode gas compositions and an additional

ohmic loss corrected polarization curve obtained with H_2–O_2. The activation overpotential η_{act} is obtained by subtracting the ohmic loss corrected H_2–O_2 polarization curve $V_{O_2} + jR_{HFR}$ from the theoretical open circuit voltage E of 1.23 V (101.3 kPa) (19.6). The ohmic overpotential η_{Ohm} was obtained by multiplying R_{HFR} with the current density j (19.7). Subtraction of the H_2/He + O_2 data V_{He+O_2} from the H_2–O_2 data V_{O_2} yielded the permeability overpotential $\eta_{MT,perm}$ (19.8) whereas the diffusion overpotential $\eta_{MT,dif}$ was obtained by deducting the H_2-air values V_{air} from the H_2/He + O_2 values V_{He+O_2} (19.9).

$$\eta_{act}(j) = E - [V_{O_2}(j) + jR_{HFR}(j)] , \quad (19.6)$$

$$\eta_{Ohm}(j) = jR_{HFR}(j) , \quad (19.7)$$

$$\eta_{MT,perm}(j) = V_{O_2}(j) - V_{He+O_2}(j) , \quad (19.8)$$

$$\eta_{MT,dif}(j) = V_{He+O_2}(j) - V_{air}(j) . \quad (19.9)$$

It is noted that $\eta_{MT,perm}$ includes a constant contribution owing to the O_2 concentration change $\eta_{MT,con}$ (the oxygen reduction reaction is first order in oxygen concentration [19.130], (19.10)) allowing separation of the concentration change contribution in the ionomer (Fig. 19.12a):

$$\eta_{MT,con} = \frac{RT}{F} \ln \frac{c_{O_2}}{c_{air}} = 45\,\text{mV} \quad (\text{at } 60\,^\circ\text{C}) , \quad (19.10)$$

where c_{O_2} and c_{air} respectively represent the O_2 concentration in the O_2 and air streams (mol/cm^3). Additional analysis refinements were discussed including a current density correction for the hydrogen crossover through the membrane [19.131] and empirical curve fitting relations with alternatives to the mass transfer polarization expression (19.5) [19.132–135].

Impedance Spectroscopy

EIS is a noninvasive diagnostic technique that separates in the frequency domain the individual effects of different processes such as proton transport in the electrolyte, interfacial charge transfer reactions and mass transport in catalyst and backing diffusion layers [19.77, 78, 136]. A small sinusoidal alternating potential or current (V_{AC}^{in},I_{AC}^{in}) is superimposed on the constant fuel cell potential or current (V_{DC}, I_{DC}) and both potential and current responses (V_{AC}^{out},I_{AC}^{out}) are recorded (Fig. 19.13). This operation is repeated for many signal frequencies. The impedance, a complex variable, is calculated by the potential and current signals ratio:

$$Z(\omega) = \frac{\Delta V}{\Delta I} = |Z|\, e^{i\phi(\omega)} = Z_{Re}(\omega) - iZ_{Im}(\omega) , \quad (19.11)$$

where Z is the impedance (Ω), ΔV is the amplitude of the potential perturbation signal (V), ΔI is the amplitude of the current response signal (A), ϕ is the phase angle, ω is the angular frequency (Hz), Z_{Re} is the real part of the impedance (Ω) and Z_{Im} is the imaginary part of the impedance (Ω). There are three necessary requirements to obtain reliable impedance measurements [19.77]. A linear behavior that implies that the perturbation signal amplitude is small in comparison to RT/F (the polarization curve is not linear, Figs. 19.11 and 19.12b), a response that is only due to the applied perturbation (the fuel cell, for instance, is operating at the steady state), and a stable response with the fuel cell returning to its original state after the perturbation is removed.

A frequency response analyzer (FRA) is used to impose the small amplitude alternating current (AC) signal to the fuel cell via the load bank. The AC voltage and current responses are processed by the FRA to determine the complex impedance for all frequencies [19.137]. Physicochemical processes occurring within the fuel cell (Fig. 19.9) have different characteristic time constants and therefore are exhibited in the spectra at different characteristic frequencies. Other options are available to modulate the fuel cell output such as with a high power potentiostat (control unit and booster).

Impedance data are displayed as the negative value of the imaginary impedance as a function of the real impedance (Nyquist plot).The Bode plot is an alternative representation of the impedance data with both the impedance magnitude and phase angle plotted as a function of the perturbation signal frequency. A representative Nyquist plot for a PEMFC is shown in Fig. 19.14. Three distinguishable, depressed semicircles are observed within the 0.1 Hz to 10 kHz frequency range [19.138, 139]. The smaller arc at high frequencies (> 1 kHz) is attributed to the transport of protons and electrons and the anode charge transfer reactions. The larger arc in the mid-frequency range (5 Hz to

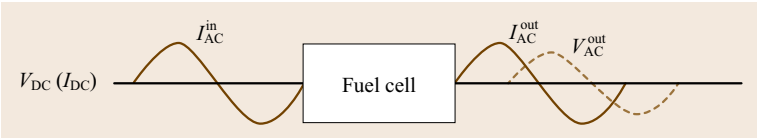

Fig. 19.13 EIS measurement principle

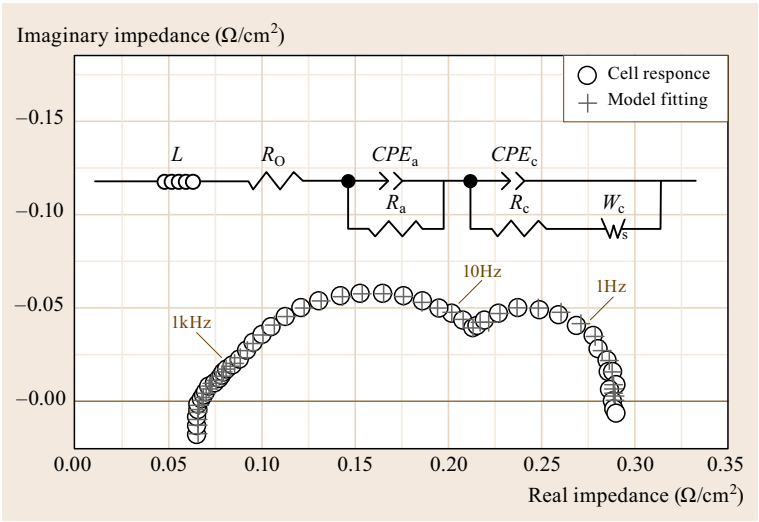

Fig. 19.14 Representative EIS for a PEMFC single cell, corresponding EEC and curve fitting results. Anode-cathode conditions: H_2/air, 2/2 stoichiometry, 100/50% relative humidity, 48.3/48.3 kPa, 80 °C, 0.6 A/cm^2, 15 mA/cm^2 AC perturbation, 0.1 Hz to 10 kHz frequency range

1 kHz) is attributed to the cathode charge transfer reactions. The remaining arc at low frequencies (0.1−5 Hz) is attributed to the reactant transport in the cathode GDE.

Equivalent electrical circuits (EEC) are extensively used to analyze impedance responses and extract physically meaningful fuel cell properties. Common electrical circuit components include resistors, capacitors, inductors, constant phase elements and Warburg elements [19.77]. An EEC for a single PEMFC is shown in Fig. 19.14; L stands for the serial inductance of the cell and system components. The electron and proton transport resistances are combined into the ohmic resistance R_O. Charge transfer resistances of the hydrogen oxidation reaction (HOR) and the oxygen reduction reaction (ORR) are represented by R_a and R_c. A finite length Warburg diffusion element W_c is included for the O_2 transport in the GDE. The H_2 diffusion resistance is negligible, eliminating the need for a Warburg element. Constant phase elements CPE_a and CPE_c represent anode and cathode double-layer capacitances with a rough catalyst layer and a nonuniform catalyst distribution [19.140]. The EEC offers an adequate representation of experimental impedance data (Fig. 19.14). Curve fitting was completed with a commercially available software (ZView, Scribner Associates) with estimated parameter errors < 5% [19.139].

Voltammetry

Cyclic voltammetry (CV) is a potentiodynamic technique for studying thermodynamic and kinetic aspects of electrochemical reactions. The potential of the working electrode (WE) is scanned linearly between two potential limits from an initial value. The current-voltage curve of the WE versus the reference electrode (RE) is referred to as the cyclic voltammogram, as shown in Fig. 19.15. The peak potential and peak currents are important characteristics [19.90, 141]. For a reversible system, the peak current j_p (A) for a reversible couple (at 25 °C) is given by the Randles–Sevcik equation

$$j_p = 2.69 \times 10^5 n^{1.5} A D^{0.5} c v^{0.5} , \qquad (19.12)$$

where A is the electrode area (cm^2), D the diffusion coefficient (cm^2/s), c the concentration (mol/cm^3) and v the potential scan rate (V/s). The corresponding peak potential separation between anode E_p^a and cathode E_p^c peak potentials (V) is

$$E_p^a - E_p^c = \frac{0.059}{n} , \qquad (19.13)$$

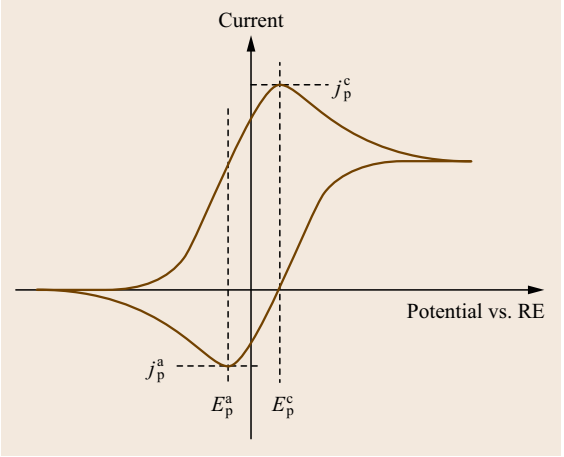

Fig. 19.15 Cyclic voltammogram for a hypothetical reaction and associated peak parameters

which is used as a criterion for a reversible or Nernstian behavior and to determine the number n of electrons transferred. In turn, the diffusion coefficient is determined using n, (19.12) and operating conditions A, c and v. The peak potentials are used to identify specific reactions. Equations (19.12) and (19.13) illustrate qualitative as well as quantitative aspects of cyclic voltammetry. Similar equations were derived for other kinetics including irreversible reactions [19.142].

A potentiostat controls the potential difference between working and reference electrodes at a desired value. An electrometer, a high-input impedance voltmeter that minimizes the reference electrode polarization, measures the voltage difference between reference and working electrodes. The potential scan rate is normally constant. The resulting current passing through the working and the counter electrodes is recorded. The potential limits and the potential scan rate are the adjustable parameters. The potential applied to the working electrode is swept back and forth between the two set voltage limits (triangular wave form).

A cyclic voltammogram for a single PEMFC is shown in Fig. 19.16. The electrode that serves as the PEMFC cathode (GDE with Pt/C as catalyst and Nafion as electrolyte) is fed with humidified N_2 and connected as the WE. The other PEMFC electrode fed with humidified H_2 serves as both counter electrode (CE) and RE. The applied WE potential is scanned between the open circuit voltage (OCV, ≈ 0 V versus the RE) and 1.2 V versus the RE. During the positive scan, the H_2 that permeates from the CE side and adsorbed H_2 on Pt ($Pt\text{-}H_{ads}$) are oxidized within the ≈ 0 to ≈ 0.4 V versus RE potential range according to

$$Pt - H_{ads} \rightarrow Pt + H^+ + e^- \,. \tag{19.14}$$

The presence of two peaks in the ≈ 0 to ≈ 0.4 V versus RE potential range is ascribed to different Pt crystallographic planes ((111) and (100) [19.143]). In the ≈ 0.4 to ≈ 0.6 V versus RE potential range, the positive current is attributed to the oxidation of the H_2 permeating through the membrane and the charging of the double-layer capacitance. Above ≈ 0.6 V versus RE, Pt oxidation takes place with the formation of Pt-OH and Pt-O species [19.144, 145]

$$Pt + H_2O \rightarrow Pt\text{-}OH + H^+ + e^- \,, \tag{19.15}$$

$$Pt\text{-}OH \rightarrow Pt\text{-}O + H^+ + e^- \,. \tag{19.16}$$

During the reverse scan, the Pt oxides are first reduced (≈ 0.77 V peak potential). Subsequently, H_2 is adsorbed on Pt (≈ 0.13 V peak potential versus RE). Below ≈ 0.1 V versus RE, H_2 evolution takes place.

The current measured in the electroinactive region around 0.4 V versus the RE is due to the charging and discharging of the double-layer capacitance associated with the Pt/ionomer interface (a constant phase element in this case, Fig. 19.14). The capacitance C (F) is determined from the charging current j_{dl} (A/cm^2) and the potential scan rate v,

$$Aj_{dl} = C\frac{dV}{dt} = Cv \,, \tag{19.17}$$

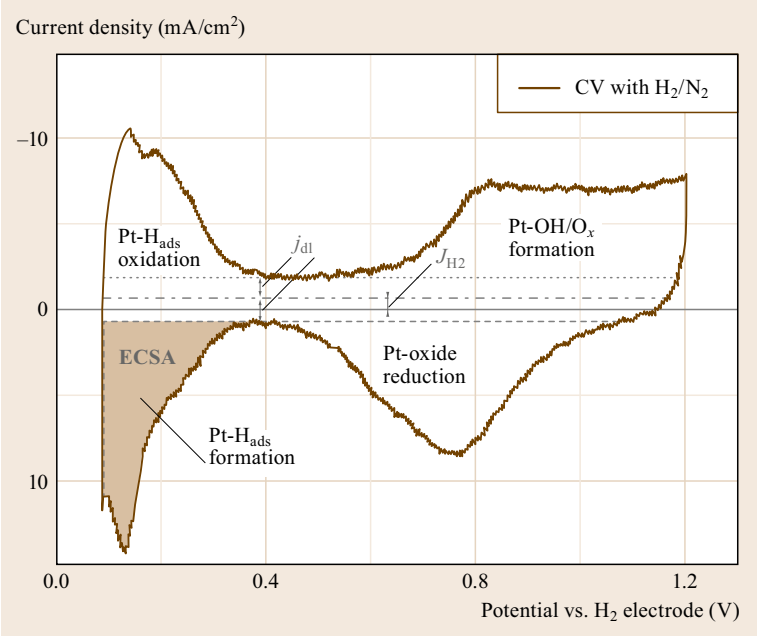

Fig. 19.16 Cyclic voltammogram of a PEMFC MEA. Counter/working electrode compartment conditions: H_2/N_2, 0.5/0.5 l/min at normal conditions, 100/100% relative humidity, 101/101 kPa, 35 °C, 20 mV/s potential scan rate

where V is the electrode potential (V versus the RE) and t the time (s). The electroinactive region around 0.4 V versus the RE is also not centered at a 0 current density because the H_2 permeating through the membrane is oxidized and contributes to a small oxidation current displacing the entire cyclic voltammogram to higher current density values. The permeating H_2 also displaces the entire cyclic voltammogram to higher potentials (diffusion cell polarization of ≈ 0.1 V).

The cyclic voltammogram is used to determine the electrochemical active surface area (ECSA or ECA) by integrating the H_2 adsorption current between ≈ 0.1 and ≈ 0.4 V versus the RE (hashed area in Fig. 19.16). The ECSA is calculated with a charge density of $210\,\mu C/cm^2$, a charge sufficient to reduce a monolayer of H_{ads} on a smooth Pt surface, and the Pt loading

$$\mathrm{ECSA} = \frac{S}{0.021mv}\,, \tag{19.18}$$

where the ECSA is in m^2/g, S is the H_2 adsorption peak area (mW/cm^2) and m the Pt loading (mg/cm^2). The ECSA is essential to compare the activity of different Pt catalyst structures. Alternatively, the H_2 oxidation peaks or CO adsorption were used to estimate the ECSA. The Pt oxides reduction peak was employed to estimate the extent of oxidation [19.146].

Linear sweep voltammetry (LSV) is similar to CV but only one scan is completed between potential limits. Furthermore the scan is completed at a much smaller scan rate equal to or less than 1 mV/s. These precautions are necessary for H_2 crossover and electrical short circuit measurements [19.89, 147] to minimize the effects of preadsorbed H_2 and the double-layer capacitance charging. A LSV curve for a H_2 crossover measurement is shown in Fig. 19.17. The WE potential is scanned at 0.1 mV/s from the ≈ 0.1 to ≈ 0.4 V versus the RE. The upper potential limit is sufficient to obtain a well-defined H_2 oxidation limiting current density. The hydrogen crossover rate J_{H_2} ($mol/s\,cm^2$) is calculated using Faraday's law

$$J_{H_2} = \frac{j_l}{nF}\,. \tag{19.19}$$

The LSV method for the determination of the H_2 crossover is an alternative to the CV method (Fig. 19.16).

In the presence of an electrical MEA short circuit, the H_2 oxidation limiting current density is not constant but rather increases at higher electrode potentials. The electrical short circuit resistance is estimated from the polarization curve slope [19.89, 147].

Other Tests

There are other diagnostic techniques that are used to characterize fuel cells but they are relatively seldom utilized. Although one of these diagnostic techniques is electrochemical, the segmented cell for current-voltage distribution across the cell active area, all the others are not. These diagnostic techniques are briefly and sequentially introduced using the high level framework of

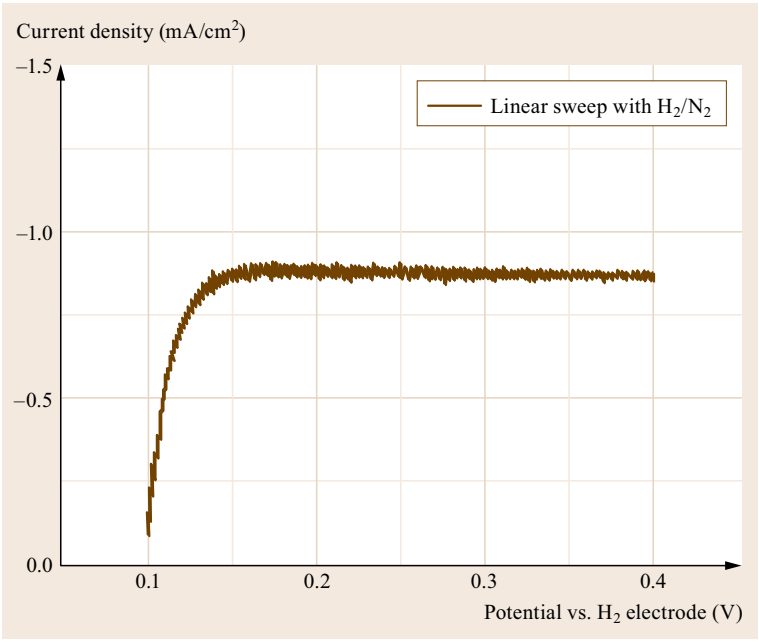

Fig. 19.17 LSV curve of a PEMFC MEA. Counter/working electrode compartment conditions: H_2/N_2, 0.5/0.5 l/min at normal conditions, 100/100% relative humidity, 101/101 kPa, 35 °C, 0.1 mV/s potential scan rate

Table 19.6 (method focus). The section concludes with the hardware-in-the-loop technique.

The consumption of reactants and the generation of products and heat in the fuel cell contribute to the variation of the species concentration and temperature along the flow field length and in turn to the uneven current-cell voltage distribution. The different gradients are impacted by cell design and are thus important to optimize performance and mitigate premature local degradation. Noninvasive measurement techniques rely on the external magnetic field [19.148] whereas invasive techniques require the electrical segregation of one or several active area components including the current collector, the bipolar plate, and the gas diffusion layer and electrode. The invasive techniques are further grouped based on manufacturing techniques including printed circuit boards [19.149] and the addition of multiple sensing or controlling elements. The latter techniques rely on the integration of high precision shunt resistors [19.150, 151], electronic loads [19.150, 152–154] or Hall sensors [19.30, 155–157]. The current-voltage distribution measurements also enable the local use of other electrochemical techniques such as impedance spectroscopy [19.30, 154, 158, 159]. Figure 19.18a illustrates local polarization curves that demonstrate the significantly uneven and interlinked performance and operating condition distributions. The kinetic and ohmic regimes are hardly impacted due to the high stoichiometries and well-humidified reactant streams (Fig. 19.11). However, the mass transfer regime at high current densities is largely modified owing to the progressive effect of product water accumulation. The cell performance decreases along the flow field length. Figure 19.18b shows the evolution of the local cell performance resulting from a temporary CO injection into the H_2 stream. The cell voltage distribution is uniform due to the high bipolar plate electrical conductivity and relatively small active area of 100 cm^2. The cell voltage distribution remains uniform during the CO injection but drops until a steady state is reached (CO adsorption on Pt decreases the catalyst active area) and recovers to its original state after the CO injection is interrupted. By contrast, the current distribution is not uniform with inlet segments relatively more affected by the CO presence with lower than 1 normalized current density values. As the total current is fixed, downstream segments have larger than 1 normalized current density values. The H_2 stream is depleted of CO along the flow field length as it progressively adsorbs on the Pt catalyst or reacts with O_2 diffusing through the membrane from the cathode compartment and creating a much weaker adsorbing CO_2 product.

Several methods are available to quantify the products generated within the fuel cell. Water mapping within the fuel cell has been the subject of extensive studies [19.11]. The most useful and less invasive methods include neutron imaging [19.80], x-ray diffraction [19.81] and residence time distribution [19.38, 39]. Liquid water exiting the fuel cell is also analyzed to obtain information about the membrane degrada-

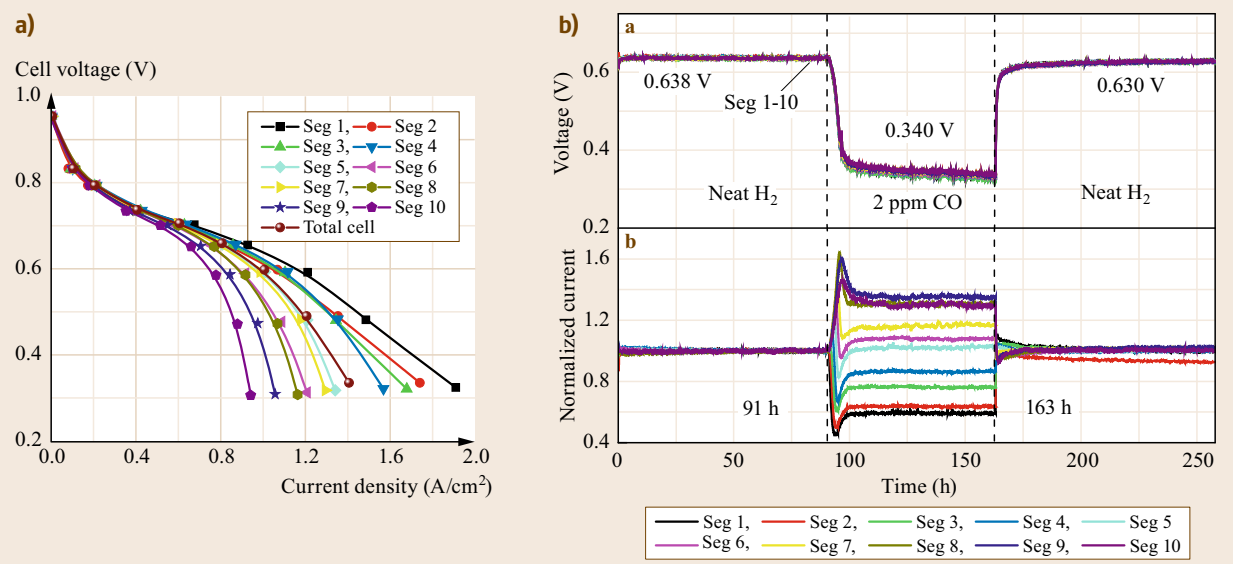

Fig. 19.18a,b Spatially distributed polarization curves for a PEMFC **(a)**. Cell voltage and normalized current density (using the initial performance) distributions at 0.8 A/cm^2 before, during and after a temporary injection of 2 ppm CO in the H_2 stream **(b)**. Anode-cathode conditions: H_2/air, 2/2 stoichiometry, 100/50% relative humidity, 48.3/48.3 kPag, 60 °C

tion rate (fluoride emission rate [19.112, 160, 161]) and assess the contaminant scavenging efficiency [19.97]. Equally, the fuel cell outlet reactant streams are sampled and analyzed to reveal the catalyst support corrosion [19.162, 163], and to establish the presence of side reactions [19.164] and the accumulation of diluents such as N_2 [19.165]. The electro-osmotic drag or number of water molecules transported with the proton in the ionomer is also quantifiable using in situ methods [19.95, 96, 166].

Some reactant properties are also quantifiable within the fuel cell. The limiting current density (Fig. 19.11) is useful to derive overall mass transfer coefficients and separate them into more fundamental contributions [19.93, 167–170]. Permeability coefficients for reactant diffusion in ionomers are also obtainable [19.89, 94]. Heat-related diagnostic methods, although available, have seldom been used. Thermocouples [19.87] as well as an infrared camera [19.88] were employed.

Fuel cell systems also need to be tested to evaluate interactions between the fuel cell and balance of plant components under conditions that mimic the expected transient operating conditions for the selected application (duty cycle). The hardware-in-the-loop technique was developed with that intent (Fig. 19.10) [19.48, 49, 121]). Figure 19.19a displays results for a fuel cell–battery hybrid power system. The total power demand (duty cycle) intermittently exceeds the nominal system power of 300 W with the excess power provided by the battery allowing the fuel cell output to remain relatively constant at ≈ 250 W. Such a control algorithm is expected to extend fuel cell life because, for example, cathode potential changes that lead to Pt catalyst active area loss by Pt dissolution and Pt nanoparticle agglomeration are minimized. This specific fuel cell stack control algorithm can only be implemented with a fuel cell–battery hybrid system. During periods when the total power demand is smaller than the nominal power (< 300 W), the excess fuel cell power is used to recharge the battery. Component sizing is also important to avoid a complete battery discharge and to maintain a reasonable battery state of charge as illustrated in Fig. 19.19a. Figure 19.19b reveals with an expanded timescale the significance of a faster test station control response time (< 100 ms) to measure and observe small and rapid fuel cell and battery dynamic changes with load demand.

19.4.3 Ex Situ Tests

A large number of ex situ tests are also available to characterize fuel cell materials. The information is used to relate freshly synthesized or aged materials parameters to fuel cell performance and degradation mechanisms. More specifically, the correlation between ex situ and in situ tests results is an issue of general relevance because in situ tests require more time and resources. There is a gap in rapid ex situ diagnostic methods that correlate with in situ tests. Tests are first analyzed on the basis of the main fuel cell performance losses (polarizations) to focus and order the discussion. Subsequently, electrochemical cells combined with spectroscopic measurements are introduced (spectroelectrochemical cells). This section leads to other material science characterization methods including spectroscopic measurements.

The rotating ring-disc electrode (RRDE) is the most popular method to obtain kinetic parameters for the main and side electrochemical reactions [19.171]. The ring-disc electrode has a geometry that consists

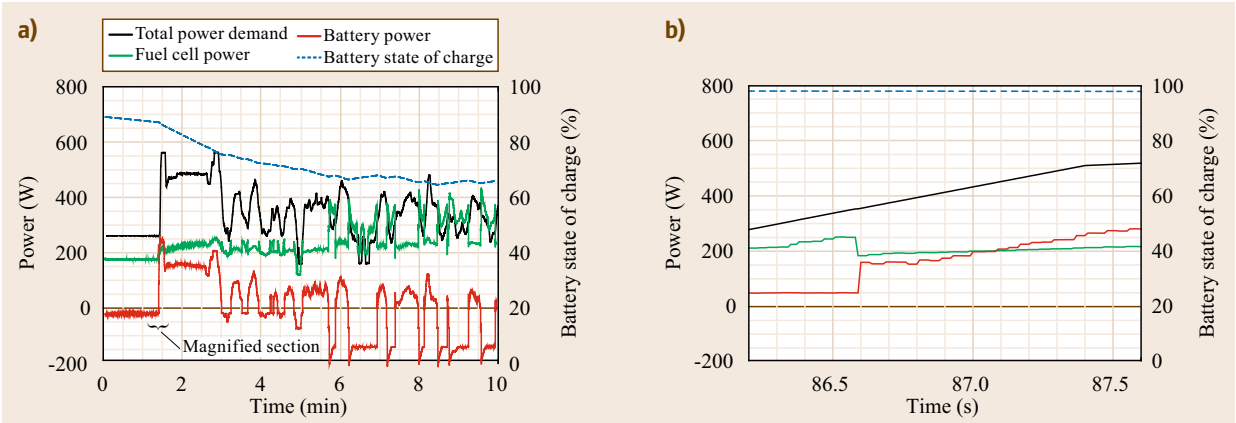

Fig. 19.19a,b Fuel cell–battery hybrid system hardware-in-the-loop duty cycle results displaying the evolution of both power levels and battery state of charge **(a)**. A magnified time scale reveals the test station response time of < 100 ms during a total power demand change that is necessary to measure and observe small and rapid fuel cell and battery dynamic changes **(b)**

of a cylinder inserted in a tube that are both fixed within an inert material and electrically isolated. All parts share the same rotation axis and only one end of the disc cylinder and ring tube assembly is electrochemically active. The ring-disc electrode rotation in an electrolyte solution is a hydrodynamic problem that has been analytically solved. For instance, the limiting current density at the disc is described by the Levich equation

$$j_l = 0.62nFAD^{2/3}\omega^{1/2}\nu^{-1/6}c\,, \tag{19.20}$$

where ν is the kinematic viscosity (cm^2/s). Equation (19.20) leads to the electroactive species diffusion coefficient if other solution properties are known. Separation of the overall current j into kinetic j_k (A/cm^2) and mass transport j_l contributions is also possible with the Koutecký–Levich equation

$$\frac{1}{j} = \frac{1}{j_k} + \frac{1}{j_l}\,. \tag{19.21}$$

A $1/j$ versus $\omega^{-1/2}$ plot yields $1/j_k$ at $\omega^{-1/2} = 0$. At the ring, reaction intermediates that are swept away from the disc surface by the hydrodynamic shearing forces are detected at a potential that is selected to create a current response. The ring potential is not necessarily equal to the disc potential. Only a fraction of the intermediates generated at the disc reach the ring and react. Therefore, in separate experiments, the collection efficiency N needs to be measured to recover the total amount of intermediates

$$N = \frac{-j_{ring}}{j_{disc}}\,. \tag{19.22}$$

A theoretical expression is available to calculate the collection efficiency [19.171]. The RRDE method is especially relevant for the oxygen reduction reaction, which leads to a small amount of peroxide that is affected by the presence of contaminants such as SO_2 [19.172]. An inverted electrode catalyst ink deposition technique was proposed and is preferred in view of an improved reproducibility and a more uniform film thickness [19.173, 174]. Figure 19.20 illustrates the reproducibility achieved for both disc polarization curves and peroxide detection. The amount of peroxide generated during oxygen reduction increases at low electrode potentials and only accounts for a few % of the disc current. However, the peroxide generated has been linked to ionomer and membrane degradation [19.175].

The ionically conductive membrane is the most electrically resistive component material of a PEMFC in comparison to Pt, C and Cu (electronic conductors). A conductivity cell is generally used to measure the membrane resistance and assess ohmic losses. The conductivity cell maintains the membrane sample in contact with a controlled atmosphere or environment and electrodes for current and voltage sensing to eliminate contact resistances (4-point electrodes method [19.176]). Direct or alternating current measurements are used to measure the membrane conductivity. However, alternating current measurements

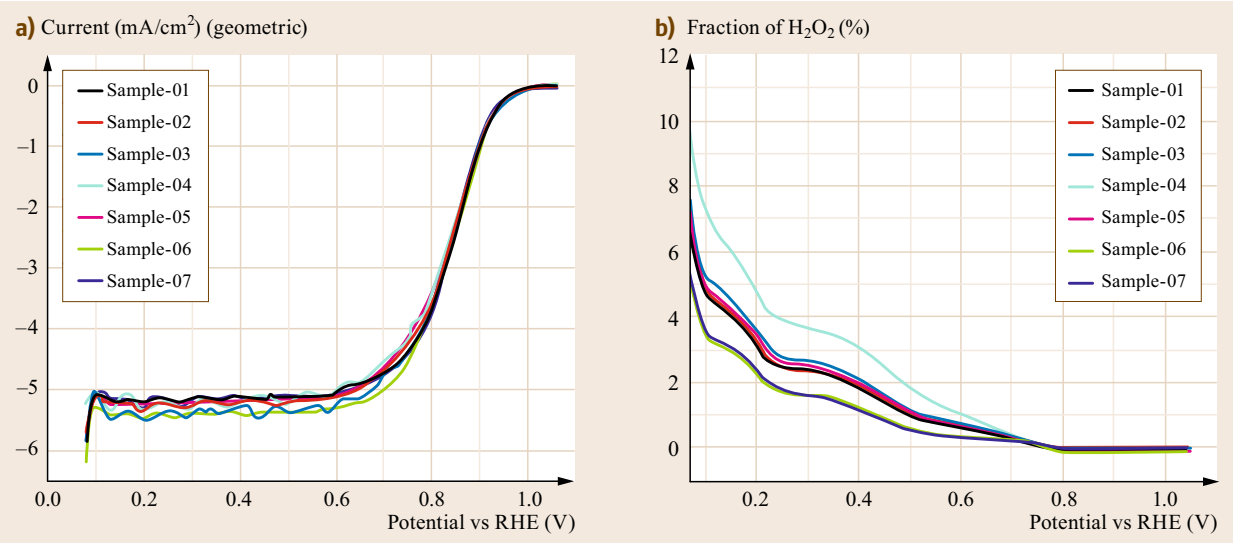

Fig. 19.20a,b Polarization curves for a catalyst ink deposited on a rotating disc electrode **(a)**, corresponding peroxide intermediate detection at the ring electrode **(b)**. Operating conditions: 0.5 M H_2SO_4 saturated with O_2, 30 °C, 20 mV/s potential scan rate, 1.2 V versus the SHE ring potential

such as impedance spectroscopy are preferred to minimize artifacts (absence of a current circulating in the membrane and electrode polarization). Through-plane measurements are also preferred because they correspond to the current and MEA stacking directions [19.61, 177]. Membrane processing affects both ionomer material isotropy and conductivity [19.178, 179]. Therefore, in-plane measurements are not preferred unless they are used for thin ionomer films with isotropic properties.

For mass transfer losses, products as well as reactants and gas and ionomer phases need to be considered. For O_2 and H_2 transport in the gas phase, Gurley measurements were used [19.180] but are not directly comparable to in situ values because the gas flow is circulated (forced convection) rather than being mostly driven by diffusion as in a PEMFC. For O_2 and H_2 diffusive transport in the ionomer phase, a diffusion cell is commonly used [19.94]. For product water vapor, diffusive transport in the gas phase is equally problematic as for O_2 and H_2. Transport of liquid water in the GDE also needs to be considered. However, this is a complex problem that has not yet been satisfactorily resolved. For H_2O transport in the ionomer phase, dynamic vapor sorption is used for diffusion control [19.181] whereas in situ measurements are preferred for electro-osmotic drag control [19.95]. Ultimately, there is a need to relate mass transfer properties to mass transfer polarizations (Sect. 19.4.2). This relationship is not as obvious to develop as for kinetic or ohmic polarizations because other parameters are needed to convert transport properties into mass transfer coefficients, which in turn are used to calculate concentration profiles and mass transfer polarizations. For example, diffusion coefficients are missing for gas-phase reactants (including tortuosity effects) whereas the thickness of the ionomer covering the catalyst is missing precluding the calculation of the concentration profiles.

Electrochemical cells used to study PEMFC reaction kinetics have been modified to include spectroscopic measurements (Raman, x-ray, infrared [19.182–185]). These seldom employed methods are useful to track in situ reaction kinetics and materials evolution that are otherwise not accessible or only obtained for pristine and aged materials.

Other ex situ tests are useful to visualize, analyze the composition, and obtain subsidiary properties for the pristine and aged fuel cell materials to support the development of enhanced and more durable materials. Visualization of surface morphology, characteristic size and other features is achieved using scanning electron microscopy (SEM), environmental scanning electron microscopy (ESEM), transmission electron microscopy (TEM), atomic force microscopy (AFM) and scanning tunneling microscopy (STM) [19.186–188]. Some of these methods have recently been adapted to obtain localized, transient information [19.189, 190]. The bulk phase composition is obtained by x-ray diffraction (XRD), x-ray absorption spectroscopy including x-ray absorption near edge structure (XANES) and extended x-ray absorption fine structure (EXAFS), x-ray radial electron density distribution (REDD) and Fourier transform infrared spectroscopy (FTIR) [19.176, 191]. The surface composition is obtained by Auger electron spectroscopy and x-ray photoelectron spectroscopy (XPS). Electronic microscopes are sometimes equipped with an energy dispersive x-ray analysis spectrometer (EDX or EDAX/EDS), an electron microprobe with wavelength dispersive x-ray spectrometer (WDS) or an energy dispersive spectrometer. Small angle x-ray scattering (SAXS) provides information relative to the ionomer structure as a function of water content (crystallinity, ion clustering, etc.). Subsidiary properties such as pore size distribution, porosity, surface tension and surface groups complement transport properties in porous media. Mercury intrusion porosimetry (MIP), through- and in-plane electrical resistivity and sessile drop are representative of the methods available to characterize GDLs and GDEs [19.192]. A similar statement applies to the ionomer with methods such as differential scanning calorimetry (DSC) and thermogravimetric analysis (TGA) [19.176].

19.5 Conclusion

Fuel cell laboratory constitutive elements were reviewed to better identify gaps including safety aspects, test stations, fuel cell components and their assembly, and in situ as well as ex situ diagnostic techniques. Several opportunities were identified to improve these areas but many other opportunities are possibly left to be discovered until further analysis is completed. For instance, interest in higher and lower operating temperatures for respectively PEMFCs and SOFCs [19.193, 194] may lead to changes in safety, operating conditions and fuel cell materials impacting both test station requirements and operating procedures. This situation equally applies to the recent interest in large-scale flow batteries with circulating liquid electrolytes [19.3]. PEMFCs and SOFCs are the favored technologies for commercialization. Other fuel cell types includ-

ing molten carbonate, phosphoric acid, direct alcohol and alkaline, which were not discussed, may similarly impact the fuel cell laboratory. Fuel cell fabrication aspects were not discussed but are important especially because state-of-the-art commercial designs are not necessarily accessible for testing by academic institutions or national laboratories. For example, the equipment necessary to process bipolar plates and MEAs is relatively extensive and expensive. Therefore, investments need to be carefully assessed especially because the technologies to obtain the best fuel cell performance are still evolving. From that standpoint, it is still unclear if molded, machined carbon-based or stamped metallic bipolar plates will lead to the best overall performance [19.62, 63].

Acknowledgments. Authors are grateful to the Office of Naval Research (award N00014-11-1-0391) and to the Hawaiian Electric Company for their ongoing support of the operations of the Hawaii Sustainable Energy Research Facility. The authors are also grateful to Junjie Ge for Fig. 19.20.

References

19.1 Breakthrough Technologies Inst. Inc.: *2011 Fuel Cell Technologies Market Report*, DOE/EE 0755 (United States Department of Energy, Washington 2012)

19.2 J. Köhler, M. Wietschel, L. Whitmarsh, D. Keles, W. Schade: Infrastructure investment for a transition to hydrogen automobiles, Technol. Forecast. Soc. Change **77**, 1237–1248 (2010)

19.3 Z. Yang, J. Zhang, M.C.W. Kintner-Meyer, X. Lu, D. Choi, J.P. Lemmon, J. Liu: Electrochemical energy storage for green grid, Chem. Rev. **111**, 3577–3613 (2011)

19.4 N. Maximova, O. Dahl: A set up of a modern analytical laboratory for wastewaters from pulp and paper industry, Chem. Soc. Rev. **36**, 1323–1349 (2007)

19.5 M.J. D'Amato, K.W. Lux, K.A. Walz, H. Walter Kerby, B. Anderegg: Introducing new learning tools into a standard classroom: A multi-tool approach to integrating fuel-cell concepts into introductory college chemistry, J. Chem. Educ. **84**, 248–252 (2007)

19.6 M. Shirkhanzadeh: Thin-layer fuel cell for teaching and classroom demonstrations, J. Chem. Educ. **86**, 324–329 (2009)

19.7 P. Lunghi, S. Ubertini: First steps towards fuel cells testing harmonisation: Procedures and parameters for single cell performance evaluation, Fuel Cells **3**, 208–219 (2004)

19.8 R. Cuccaro, M. Lucariello, A. Battaglia, A. Graizzaro: Research of a HySyLab internal standard procedure for single PEMFC, Int. J. Hydrog. Energy **33**, 3159–3166 (2008)

19.9 T. Malkow, A. Saturnio, A. Pilenga, G. De Marco, M. Honselaar, G. Tsotridis: Assessment of PEFC performance by applying harmonized testing procedure, Int. J. Energy Res. **35**, 1075–1089 (2011)

19.10 G. De Moor, C. Bas, F. Lesage, A. Sophie Danérol, E. Claude, E. Rossinot, M. Paris, L. Flandin, N. Dominique Albérola: Understanding the degradation of MEA in PEMFC: Definition of structural markers and comparison between laboratory and on-site ageing, J. Appl. Polym. Sci. **120**, 3501–3510 (2011)

19.11 J. St-Pierre: PEMFC in-situ liquid-water-content monitoring status, J. Electrochem. Soc. **154**, B724–B731 (2007)

19.12 S.A. Freunberger, M. Reum, J. Evertz, A. Wokaun, F.N. Büchi: Measuring the current distribution in PEFCs with sub-millimeter resolution I. methodology, J. Electrochem. Soc. **153**, A2158–A2165 (2006)

19.13 J. St-Pierre: PEMFC contamination model: Foreign cation exchange with ionomer protons, J. Power Sources **196**, 6274–6283 (2011)

19.14 J. St-Pierre: PEMFC contaminant tolerance limit-foreign cations in ionomers, Int. J. Hydrog. Energy **36**, 5527–5535 (2011)

19.15 A.M. Sapienza: *Managing Scientists: Leadership Strategies in Scientific Research*, 2nd edn. (Wiley-Liss, Hoboken 2004) pp. 31–33

19.16 M. Reijalt: Hydrogen and fuel cell education in Europe: From when? and where? to here! and now!, J. Clean. Prod. **18**, S112–S117 (2010)

19.17 Fuel Cell Today, http://www.fuelcelltoday.com

19.18 J. Glassey, S. Haile: Sustainability in chemical engineering curriculum, Int. J. Sustain. High. Educ. **13**, 354–364 (2012)

19.19 L. Diener: Selected online resources for teaching about alternative energy, J. Chem. Educ. **89**, 950–952 (2012)

19.20 R. Wünschiers, P. Lindblad: Hydrogen in education – A biological approach, Int. J. Hydrog. Energy **27**, 1131–1140 (2002)

19.21 B. Briggs, T. Mitton, R. Smith, T. Magnuson: Teaching cellular respiration and alternate energy sources with a laboratory exercise developed by a scientist-teacher partnership, Am. Biol. Teach. **71**, 164–167 (2009)

19.22 A. Serov, C. Kwak: Direct hydrazine fuel cells: A review, Appl. Catal. B **98**, 1–9 (2010)

19.23 A. Serov, C. Kwak: Progress in development of direct dimethyl ether fuel cells, Appl. Catal. B **91**, 1–10 (2009)

19.24 F. Yang, K. Cheng, X. Liu, S. Chang, J. Yin, C. Du, L. Du, G. Wang, D. Cao: Direct peroxide-peroxide fuel cell – Part 2: Effects of conditions on the performance, J. Power Sources **217**, 569–573 (2012)

19.25 J. Ma, N.A. Choudhury, Y. Sahai: A comprehensive review of direct borohydride fuel cells, Renew. Sustain. Energy Rev. **14**, 183–199 (2010)

19.26 G.R. Astbury: A review of the properties and hazards of some alternative fuels, Process Saf. Environ. Prot. **86**, 397–414 (2008)

19.27 Compressed Gas Association: *Handbook of Compressed Gases*, 4th edn. (Springer, Berlin, Heidelberg 1999)

19.28 C.H. Rivkin (Ed.): *The NFPA Guide to Gas Safety* (National Fire Protection Association, Quincy 2005)

19.29 Y.W. Rho, S. Srinivasan, Y.T. Kho: Mass transport phenomena in proton exchange membrane fuel cells using O_2/He, O_2/Ar, and O_2/N_2 mixtures II: Theoretical analysis, J. Electrochem. Soc. **141**, 2089–2096 (1994)

19.30 T.V. Reshetenko, G. Bender, K. Bethune, R. Rocheleau: Systematic study of back pressure and anode stoichiometry effects on spatial PEMFC performance distribution, Electrochimica Acta **56**, 8700–8710 (2011)

19.31 H.D. Beeson, S.R. Smith, W.F. Stewart (Eds.): *Safe Use of Oxygen and Oxygen Systems: Handbook for Design, Operation, and Maintenance*, 2nd edn. (ASTM Intl., West Conshohocken 2007)

19.32 D.K. Berry: Air toxics in the United States – Magnitude of the problem and strategy for control, Toxicol. Ind. Health **6**, 1–12 (1990)

19.33 P.M. Lemieux, C.C. Lutes, D.A. Santoianni: Emissions of organic air toxics from open burning: A comprehensive review, Prog. Energy Combust. Sci. **30**, 1–32 (2004)

19.34 G.M. Woodall, R.L. Smith: The air toxics health effects database (ATHED), Toxicol. Appl. Pharmacol. **233**, 20–24 (2008)

19.35 J. St-Pierre, M.S. Angelo, Y. Zhai: Focusing research by developing performance related selection criteria for PEMFC contaminants, Electrochem. Soc. Trans. **41**(1), 279–286 (2011)

19.36 R. Borup, J. Meyers, B. Pivovar, Y.S. Kim, R. Mukundan, N. Garland, D. Myers, M. Wilson, F. Garzon, D. Wood, P. Zelenay, K. More, K. Stroh, T. Zawodzinski, J. Boncella, J.E. McGrath, M. Inaba, K. Miyatake, M. Hori, K. Ota, Z. Ogumi, S. Miyata, A. Nishikata, Z. Siroma, Y. Uchimoto, K. Yasuda, K.-I. Kimijima, N. Iwashita: Scientific aspects of polymer electrolyte fuel cell durability and degradation, Chem. Rev. **107**, 3904–3951 (2007)

19.37 C.S. Macomber, J. Christ, H. Wang, B. Pivovar, H.N. Dinh: Characterizing leachant contaminants from fuel cell assembly aids, a prelude to effects on performance, Electrochem. Soc. Trans. **50**(2), 603–618 (2012)

19.38 J. Diep, D. Kiel, J. St-Pierre, A. Wong: Development of a residence time distribution method for proton exchange membrane fuel cell evaluation, Chem. Eng. Sci. **62**, 846–857 (2007)

19.39 J. St-Pierre, A. Wong, J. Diep, D. Kiel: Demonstration of a residence time distribution method for proton exchange membrane fuel cell evaluation, J. Power Sources **164**, 196–202 (2007)

19.40 H.S. Fogler: *Elements of Chemical Reaction Engineering*, 4th edn. (Prentice Hall, Upper Saddle River 2006) p. 871

19.41 D. Roberts: 50-V shock hazard threshold, IEEE Trans. Ind. Appl. **46**, 102–107 (2010)

19.42 T.B. Reddy (Ed.): *Linden's Handbook of Batteries*, 4th edn. (McGraw-Hill, New York 2011), Chap. 5

19.43 S. Kreitmeier, M. Michiardi, A. Wokaun, F.N. Büchi: Factors determining the gas crossover through pinholes in polymer electrolyte fuel cell membranes, Electrochimica Acta **80**, 240–247 (2012)

19.44 A.Z. Weber: Gas-crossover and membrane-pinhole effects in polymer-electrolyte fuel cells, J. Electrochem. Soc. **155**, B521–B531 (2008)

19.45 J. Zhang, J. Lee: A review on prognostics and health monitoring of Li-ion battery, J. Power Sources **196**, 6007–6014 (2011)

19.46 J. St-Pierre: Air impurities. In: *Polymer Electrolyte Fuel Cell Durability*, ed. by F.N. Büchi, M. Inaba, T.J. Schmidt (Springer, Berlin, Heidelberg 2009) pp. 289–321

19.47 K. Promislow, J. St-Pierre, B. Wetton: A simple, analytic model of polymer electrolyte membrane fuel cell anode recirculation at operating power including nitrogen crossover, J. Power Sources **196**, 10050–10056 (2011)

19.48 G. Randolf, R.M. Moore: Test system design for hardware-in-loop evaluation of PEM fuel cells and auxiliaries, J. Power Sources **158**, 392–396 (2005)

19.49 R.M. Moore, K.H. Hauer, G. Randolf, M. Virji: Fuel cell hardware-in-loop, J. Power Sources **162**, 302–308 (2006)

19.50 D. Stolten, T. Grube (Eds.): *18th World Hydrogen Energy Conference–WHEC 2010, Parallel Sessions Book 6: Stationary Applications/Transportation Applications* (Forchungszentrum Jülich, Jülich 2010) pp. 115–120

19.51 S. Begot, F. Harel, J.M. Kauffmann: Design and validation of a 2 kW-fuel cell test bench for subfreezing studies, Fuel Cells **8**, 23–32 (2008)

19.52 T.A. Zawodzinski Jr., C. Derouin, S. Radzinski, R.J. Sherman, V.T. Smith, T.E. Springer, S. Gottesfeld: Water uptake by and transport through Nafion 117 membranes, J. Electrochem. Soc. **140**, 1041–1047 (1993)

19.53 F. Barbir: *PEM Fuel Cells: Theory and Practice* (Elsevier, Amsterdam 2005) pp. 55–57

19.54 S. Pischinger, O. Lang: Air-supply components. In: *Handbook of Fuel Cells*, Vol. 4, ed. by W. Vielstich, A. Lamm, H.A. Gasteiger (Wiley, New York 2003) pp. 727–741

19.55 M.J. Lampinen, M. Fomino: Analysis of free energy and entropy changes for half-cell reactions, J. Electrochem. Soc. **140**, 3537–3546 (1993)

19.56 J. St-Pierre, J. Roberts, K. Colbow, S. Campbell, A. Nelson: PEMFC operational and design strategies for sub zero environments, J. New Mater. Electrochem. Syst. **8**, 163–176 (2005)

19.57 R. Hanke-Rauschenbach, M. Mangold, K. Sundmacher: Bistable current-voltage characteristics of PEM fuel cells operated with reduced feed

stream humidification, J. Electrochem. Soc. **155**, B97–B107 (2008)
19.58 T. Kadyk, S. Kirsch, R. Hanke-Rauschenbach, K. Sundmacher: Autonomous potential oscillations at the Pt anode of a polymer electrolyte membrane fuel cell under CO poisoning, Electrochimica Acta **56**, 10593–10602 (2011)
19.59 A. Taniguchi, T. Akita, K. Yasuda, Y. Miyazaki: Analysis of electrocatalyst degradation in PEMFC caused by cell reversal during fuel starvation, J. Power Sources **130**, 42–49 (2004)
19.60 Anonymous: *Fuel Cell Testing – The NI Way*, White Paper 2759 (National Instruments, Austin 2012)
19.61 J. St-Pierre: Stacks. In: *Encyclopedia of Electrochemical Power Sources*, Vol. 2, ed. by J. Garche, C. Dyer, P. Moseley, Z. Ogumi, D. Rand, B. Scrosati (Elsevier, Amsterdam 2009) pp. 879–889
19.62 V. Mehta, J.S. Cooper: Review and analysis of PEM fuel cell design and manufacturing, J. Power Sources **114**, 32–53 (2003)
19.63 H. Tawfik, Y. Hung, D. Mahajan: Metal bipolar plates for PEM fuel cell – A review, J. Power Sources **163**, 755–767 (2007)
19.64 J.H. Nam, M. Kaviany: Effective diffusivity and water-saturation distribution in single- and two-layer PEMFC diffusion medium, Int. J. Heat Mass Transf. **46**, 4595–4611 (2003)
19.65 G. Lin, T. Van Nguyen: Effect of thickness and hydrophobic polymer content of the gas diffusion layer on electrode flooding level in a PEMFC, J. Electrochem. Soc. **152**, A1942–A1948 (2005)
19.66 J. St-Pierre: Overview performance and operational conditions. In: *Encyclopedia of Electrochemical Power Sources*, Vol. 2, ed. by J. Garche, C. Dyer, P. Moseley, Z. Ogumi, D. Rand, B. Scrosati (Elsevier, Amsterdam 2009) pp. 901–911
19.67 S.-Y. Ahn, S.-J. Shin, H.Y. Ha, S.-A. Hong, Y.-C. Lee, T.W. Lim, I.-H. Oh: Performance and lifetime analysis of the kW-class PEMFC stack, J. Power Sources **106**, 295–303 (2002)
19.68 I. Nazarov, K. Promislow: The impact of membrane constraint on PEM fuel cell water management, J. Electrochem. Soc. **154**, B623–B630 (2007)
19.69 C.J. Netwall, B.D. Gould, J.A. Rodgers, N.J. Nasello, K.E. Swider-Lyons: Decreasing contact resistance in proton-exchange membrane fuel cells with metal bipolar plates, J. Power Sources **227**, 137–144 (2013)
19.70 R.K. Jain, H.C. Triandis: *Management of Research and Development Organizations: Managing the Unmanageable*, 2nd edn. (Wiley, New York 1997)
19.71 E. Sadeghia, N. Djilali, M. Bahrami: Effective thermal conductivity and thermal contact resistance of gas diffusion layers in proton exchange membrane fuel cells. Part 2: Hysteresis effect under cyclic compressive load, J. Power Sources **195**, 8104–8109 (2010)
19.72 O. Burheim, P.J.S. Vie, J.G. Pharoah, S. Kjelstrup: Ex-situ measurements of through-plane thermal conductivities in a polymer electrolyte fuel cell, J. Power Sources **195**, 249–256 (2010)
19.73 M. Hamour, J.P. Garnier, J.C. Grandidier, A. Ouibrahim, S. Martemianov: Thermal-conductivity characterization of gas diffusion layer in proton exchange membrane fuel cells and electrolyzers under mechanical loading, Int. J. Thermophys. **32**, 1025–1037 (2011)
19.74 R. Zaffou, J.S. Yi, H.R. Kunz, J.M. Fenton: Temperature-driven water transport through membrane electrode assembly of proton exchange membrane fuel cells, Electrochem. Solid-State Lett. **9**, A418–A422 (2006)
19.75 K. Promislow, J. Stockie, B. Wetton: A sharp interface reduction for multiphase transport in a porous fuel cell electrode, Proc. R. Soc. A **462**, 789–816 (2006)
19.76 K. Promislow, B. Wetton: A simple, mathematical model of thermal coupling in fuel cell stacks, J. Power Sources **150**, 129–135 (2005)
19.77 E. Barsoukov, J.R. MacDonald (Eds.): *Impedance Spectroscopy: Theory, Experiment and Applications*, 2nd edn. (Wiley, New York 2005)
19.78 M.E. Orazem, B. Tribollet: *Electrochemical Impedance Spectroscopy* (Wiley, New York 2008)
19.79 F.N. Büchi, A. Marek, G.G. Scherer: In-situ membrane resistance measurements in polymer electrolyte fuel cells by fast auxiliary current pulses, J. Electrochem. Soc. **142**, 1895–1901 (1995)
19.80 R. Mukundan, R.L. Borup: Visualising liquid water in PEM fuel cells using neutron imaging, Fuel Cells **9**, 499–505 (2009)
19.81 A. Isopo, F. Nobili, V.R. Albertini: Energy dispersive x-ray diffraction applied to laboratory investigation on proton exchange membrane water content in working fuel cells, Fuel Cells **12**, 800–808 (2012)
19.82 K. Tüber, D. Pócza, C. Hebling: Visualization of water buildup in the cathode of a transparent PEM fuel cell, J. Power Sources **124**, 403–414 (2003)
19.83 X.G. Yang, F.Y. Zhang, A.L. Lubawy, C.Y. Wang: Visualization of liquid water transport in a PEFC, Electrochem. Solid-State Lett. **7**, A408–A411 (2004)
19.84 A.P. Young, J. Stumper, S. Knights, E. Gyenge: Ionomer degradation in polymer electrolyte membrane fuel cells, J. Electrochem. Soc. **157**, B425–B436 (2010)
19.85 G. Bender, M. Angelo, K. Bethune, S. Dorn, T. Thampan, R. Rocheleau: Method using gas chromatography to determine the molar flow balance for proton exchange membrane fuel cells exposed to impurities, J. Power Sources **193**, 713–722 (2009)
19.86 G.A. Schuler, A. Wokaun, F.N. Büchi: Local online gas analysis in PEFC using tracer gas concepts, J. Power Sources **195**, 1647–1656 (2010)
19.87 P.J.S. Vie, S. Kjelstrup: Thermal conductivities from temperature profiles in the polymer electrolyte fuel cell, Electrochimica Acta **49**, 1069–1077 (2004)
19.88 M. Matian, A.J. Marquis, N.P. Brandon: Application of thermal imaging to validate a heat transfer model for polymer electrolyte fuel cells, Int. J. Hydrog. Energy **35**, 12308–12316 (2010)

19.89 S.S. Kocha, J.D. Yang, J.S. Yi: Characterization of gas crossover and its implications in PEM fuel cells, Am. Inst. Chem. Eng. J. **52**, 1916–1925 (2006)

19.90 W. Vielstich: Cyclic voltammetry. In: *Handbook of Fuel Cells*, Vol. 2, ed. by W. Vielstich, A. Lamm, H.A. Gasteiger (Wiley, New York 2003) pp. 153–162

19.91 R.W. Lindström, K. Kortsdottir, M. Wesselmark, A. Oyarce, C. Lagergren, G. Lindbergh: Active area determination of porous Pt electrodes used in polymer electrolyte fuel cells: Temperature and humidity effects, J. Electrochem. Soc. **157**, B1795–B1801 (2010)

19.92 M. Inaba, T. Kinumoto, M. Kiriake, R. Umebayashi, A. Tasaka, Z. Ogumi: Gas crossover and membrane degradation in polymer electrolyte fuel cells, Electrochimica Acta **51**, 5746–5753 (2006)

19.93 T.V. Reshetenko, J. St-Pierre: PEMFC GDE oxygen mass transport coefficient separation with different gas diluents, Electrochem. Soc. Trans. **50**(2), 549–555 (2012)

19.94 K. Broka, P. Ekdunge: Oxygen and hydrogen permeation properties and water uptake of Nafion 117 membrane and recast film for PEM fuel cell, J. Appl. Electrochem. **27**, 117–123 (1997)

19.95 K.-H. Choi, D.-H. Peck, C.S. Kim, D.-R. Shin, T.-H. Lee: Water transport in polymer membranes for PEMFC, J. Power Sources **86**, 197–201 (2000)

19.96 Z. Peng, A. Morin, P. Huguet, P. Schott, J. Pauchet: In-situ measurement of electroosmotic drag coefficient in nafion membrane for the PEMFC, J. Phys. Chem. B **115**, 12835–12844 (2011)

19.97 B. Wetton, J. St-Pierre: Liquid water scavenging of PEMFC contaminants, Electrochem. Soc. Trans. **50**(2), 649–657 (2012)

19.98 J. St-Pierre: Section preface. In: *Device and Materials Modeling in PEM Fuel Cells*, ed. by S.J. Paddison, K.S. Promislow (Springer, Berlin, Heidelberg 2009) pp. 3–17

19.99 G.-S. Kim, J. St-Pierre, K. Promislow, B. Wetton: Electrical coupling in proton exchange membrane fuel cell stacks, J. Power Sources **152**, 210–217 (2005)

19.100 P.A.C. Chang, J. St-Pierre, J. Stumper, B. Wetton: Flow distribution in proton exchange membrane fuel cell stacks, J. Power Sources **162**, 340–355 (2006)

19.101 P. Berg, A. Çağlar, K. Promislow, J. St-Pierre, B. Wetton: Electrical coupling in proton exchange membrane fuel cell stacks: Mathematical and computational modelling, IMA J. Appl. Math. **71**, 241–261 (2006)

19.102 X. Cheng, B. Yi, M. Han, J. Zhang, Y. Qiao, J. Yu: Investigation of platinum utilization and morphology in catalyst layer of polymer electrolyte fuel cells, J. Power Sources **79**, 75–81 (1999)

19.103 Z. Qi, A. Kaufman: Activation of low temperature PEM fuel cells, J. Power Sources **111**, 181–184 (2002)

19.104 Z. Xu, Z. Qi, A. Kaufman: Activation of proton-exchange membrane fuel cell via CO oxidation stripping, J. Power Sources **156**, 281–283 (2006)

19.105 H. Tomioka, Y. Hashimasa, N. Yoshimura, M. Akai, S. Watanabe: JARI standard single cell testing protocol, JARI Res. J. **28**, 247–252 (2006)

19.106 Anonymous: *Procedure for Performing PEM Single Cell Testing* (Florida Solar Energy Center, Cocoa 2009)

19.107 T. Malkow, G. De Marco, A. Pilenga, M. Honselaar, G. Tsotridis, S. Escribano, L. Antoni, R. Reißner, O. Thalau, E. Sitters, G. Heinz: *Testing the Voltage and the Power as a Function of the Current Density Following a Dynamic Profile Versus Time–Dynamic Load Cycling Ageing Test for a PEFC Single Cell, Test Module PEFC SC 5-7* (European Commission Joint Research Centre, Institute for Energy, Petten 2010)

19.108 G. Bender, M. Angelo, K. Bethune, R. Rocheleau: Quantitative analysis of the performance impact of low-level carbon monoxide exposure in proton exchange membrane fuel cells, J. Power Sources **228**, 159–169 (2013)

19.109 J. St-Pierre, D.P. Wilkinson, S. Knights, M.L. Bos: Relationships between water management, contamination and lifetime degradation in PEFC, J. New Mater. Electrochem. Syst. **3**, 99–106 (2000)

19.110 J. St-Pierre, N. Jia: Successful demonstration of Ballard PEMFCs for space shuttle applications, J. New Mater. Electrochem. Syst. **5**, 263–271 (2002)

19.111 S.D. Knights, K.M. Colbow, J. St-Pierre, D.P. Wilkinson: Aging mechanisms and lifetime, PEFC and DMFC, J. Power Sources **127**, 127–134 (2004)

19.112 J. Xie, D.L. Wood, D.M. Wayne, T.A. Zawodzinski, P. Atanassov, R.L. Borup: Durability of PEFCs at high humidity conditions, J. Electrochem. Soc. **152**, A104–A113 (2005)

19.113 S.J.C. Cleghorn, D.K. Mayfield, D.A. Moore, J.C. Moore, G. Rusch, T.W. Sherman, N.T. Sisofo, U. Beuscher: A polymer electrolyte fuel cell life test: 3 years of continuous operation, J. Power Sources **158**, 446–454 (2006)

19.114 D. Liu, S. Case: Durability study of proton exchange membrane fuel cells under dynamic testing conditions with cyclic current profile, J. Power Sources **162**, 521–531 (2006)

19.115 R. Borup, J. Davey, F. Garzon, D. Wood, P. Welch, K. More: PEM fuel cell durability with transportation transient operation, Electrochem. Soc. Trans. **3**(1), 879–886 (2006)

19.116 R. Lin, B. Li, Y.P. Hou, J.M. Ma: Investigation of dynamic driving cycle effect on performance degradation and micro-structure change of PEM fuel cell, Int. J. Hydrog. Energy **34**, 2369–2376 (2009)

19.117 B. Li, R. Lin, D. Yang, J. Ma: Effect of driving cycle on the performance of PEM fuel cell and microstructure of membrane electrode assembly, Int. J. Hydrog. Energy **35**, 2814–2819 (2010)

19.118 X.-Z. Yuan, H. Li, S. Zhang, J. Martin, H. Wang: A review of polymer electrolyte membrane fuel cell durability test protocols, J. Power Sources **196**, 9107–9116 (2011)

19.119 S.J. Bae, S.-J. Kim, J.I. Park, C.W. Park, J.-H. Lee, I. Song, N. Lee, K.-B. Kim, J.-Y. Park: Lifetime prediction of a polymer electrolyte membrane fuel cell via an accelerated startup-shutdown cycle test, Int. J. Hydrog. Energy **37**, 9775–9781 (2012)

19.120 T.-C. Jao, G.-B. Jung, S.-C. Kuo, W.-J. Tzeng, A. Su: Degradation mechanism study of PTFE/Nafion membrane in MEA utilizing an accelerated degradation technique, Int. J. Hydrog. Energy **37**, 13623–13630 (2012)

19.121 T.H. Bradley, B.A. Moffitt, D.N. Mavris, T.F. Fuller, D.E. Parekh: Hardware-in-the-loop testing of a fuel cell aircraft powerplant, J. Propuls. Power **25**, 1336–1344 (2009)

19.122 H. Schulenburg, J. Durst, E. Müller, A. Wokaun, G.G. Scherer: Real surface area measurements of Pt_3Co/C catalysts, J. Electroanal. Chem. **642**, 52–60 (2010)

19.123 H.A. Gasteiger, S.S. Kocha, B. Sompalli, F.T. Wagner: Activity benchmarks and requirements for Pt, Pt-alloy, and non-Pt oxygen reduction catalysts for PEMFCs, Appl. Catal. B **56**, 9–35 (2005)

19.124 S.S. Kocha: Principles of MEA preparation. In: *Handbook of Fuel Cells*, Vol. 3, ed. by W. Vielstich, H.A. Gasteiger, A. Lamm (Wiley, New York 2003) pp. 538–565

19.125 F. Barbir: *PEM Fuel Cells: Theory and Practice* (Elsevier, Amsterdam 2005) pp. 449–452

19.126 M.V. Williams, H.R. Kunz, J.M. Fenton: Analysis of polarization curves to evaluate polarization sources in hydrogen/air PEM fuel cells, J. Electrochem. Soc. **152**, A635–A644 (2005)

19.127 F. Barbir: *PEM Fuel Cells: Theory and Practice* (Elsevier, Amsterdam 2005) pp. 45–47

19.128 T.R. Ralph, M.P. Hogarth: Catalysis for low temperature fuel cells Part I: The cathode challenges, Platin. Met. Rev. **46**, 3–14 (2002)

19.129 D.R. Lide (Ed.): *CRC Handbook of Chemistry and Physics*, 89th edn. (CRC, Boca Raton 2008) p. 6-214

19.130 K. O'Neil, J.P. Meyers, R.M. Darling, M.L. Perry: Oxygen gain analysis for proton exchange membrane fuel cells, Int. J. Hydrog. Energy **37**, 373–382 (2012)

19.131 K.C. Neyerlin, W. Gu, J. Jorne, H.A. Gasteiger: Determination of catalyst unique parameters for the oxygen reduction reaction in a PEMFC, J. Electrochem. Soc. **153**, A1955–A1963 (2006)

19.132 J. Kim, S.-M. Lee, S. Srinivasan, C.E. Chamberlin: Modeling of proton-exchange membrane fuel-cell performance with an empirical-equation, J. Electrochem. Soc. **142**, 2670–2674 (1995)

19.133 G. Squadrito, G. Maggio, E. Passalacqua, F. Lufrano, A. Patti: An empirical equation for polymer electrolyte fuel cell (PEFC) behaviour, J. Appl. Electrochem. **29**, 1449–1455 (1999)

19.134 D. Chu, R. Jiang, C. Walker: Analysis of PEM fuel cell stacks using an empirical current-voltage equation, J. Appl. Electrochem. **30**, 365–370 (2000)

19.135 L. Pisani, G. Murgia, M. Valentini, B. D'Aguanno: A new semi-empirical approach to performance curves of polymer electrolyte fuel cells, J. Power Sources **108**, 192–203 (2002)

19.136 A. Bard, L. Faulkner: *Electrochemical Methods: Fundamentals and Applications*, 2nd edn. (Wiley, New York 2000) pp. 383–388

19.137 K.R. Cooper, M. Smith: Electrical test methods for on-line fuel cell ohmic resistance measurement, J. Power Sources **160**, 1088–1095 (2006)

19.138 D. Malevich, E. Halliop, B.A. Peppley, J.G. Pharoah, K. Karan: Investigation of charge-transfer and mass-transport resistances in PEMFCs with microporous layer using electrochemical impedance spectroscopy, J. Electrochem. Soc. **156**, B216–B224 (2009)

19.139 Y. Zhai, K. Bethune, S. Dorn, G. Bender, R. Rocheleau: Analysis of the SO_2 contamination effect on the oxygen reduction reaction in PEMFCs by electrochemical impedance spectroscopy, J. Electrochem. Soc. **159**, B524–B530 (2012)

19.140 J.B. Jorcin, M.E. Orazem, N. Pébère, B. Tribollet: CPE analysis by local electrochemical impedance spectroscopy, Electrochim. Acta **51**, 1473–1479 (2006)

19.141 A.J. Bard, L.R. Faulkner: *Electrochemical Methods: Fundamentals and Applications*, 2nd edn. (Wiley, New York 2001) pp. 239–243

19.142 J. Wang: *Analytical Electrochemistry*, 3rd edn. (Wiley, New York 2006)

19.143 Y. Sun, Y. Dai, Y. Liu, S. Chen: A rotating disk electrode study of the particle size effects of Pt for the hydrogen oxidation reaction, Phys. Chem. Chem. Phys. **14**, 2278–2285 (2012)

19.144 R.M. Darling, J.P. Meyers: Kinetic model of platinum dissolution in PEMFCs, J. Electrochem. Soc. **150**, A1523–A1527 (2003)

19.145 Y. Gu, J. St-Pierre, A. Joly, R. Goeke, A. Datye, P. Atanassov: Aging Studies of Pt/glassy carbon model electrocatalysts, J. Electrochem. Soc. **156**, B485–B492 (2009)

19.146 H. Xu, R. Kunz, J.M. Fenton: Investigation of platinum oxidation in PEM fuel cells at various relative humidities, Electrochem. Solid-State Lett. **10**, B1–B5 (2007)

19.147 K.R. Cooper: In-situ PEM fuel cell: Fuel crossover and electrical short circuit measurement, Fuel Cells **8**, 34–35 (2008)

19.148 K.-H. Hauer, R. Potthast, T. Wüster, D. Stolten: Magnetotomography – A new method for analysing fuel cell performance and quality, J. Power Sources **143**, 67–74 (2005)

19.149 S. Cleghorn, C.R. Derouin, M.S. Wilson, S. Gottesfeld: A printed circuit board approach to measuring current distribution in a fuel cell, J. Appl. Electrochem. **28**, 663–672 (1998)

19.150 J. Stumper, S.A. Campbell, D.P. Wilkinson, M.C. Johnson, M. Davis: In-situ methods for the determination of current distributions in PEM fuel cells, Electrochimica Acta **43**, 3773–3783 (1998)

19.151 M. Noponen, T. Mennola, M. Mikkola, T. Hottinen, P. Lund: Measurement of current distribution in a free-breathing PEMFC, J. Power Sources **106**, 304–312 (2002)

19.152 N. Rajalakshmi, M. Raja, K.S. Dhathathereyan: Evaluation of current distribution in a proton exchange membrane fuel cell by segmented cell approach, J. Power Sources **112**, 331–336 (2002)

19.153 M.M. Mench, C.Y. Wang: An in-situ method for determination of current distribution in PEM fuel cells applied to a direct methanol fuel cell, J. Electrochem. Soc. **150**, A79–A85 (2003)

19.154 D.J.L. Brett, S. Atkins, N.P. Brandon, V. Vesivic, N. Vasileiadis, A. Kucernak: Localized impedance measurements along a single channel of a solid polymer fuel cell, Electrochem. Solid-State Lett. **6**, A63–A66 (2003)

19.155 C. Wieser, A. Helmbold, E. Gülzow: A new technique for two-dimensional current distribution measurements in electrochemical cells, J. Appl. Electrochem. **30**, 803–807 (2000)

19.156 G. Bender, M.S. Wilson, T.A. Zawodzinski: Further refinements in the segmented cell approach to diagnosing performance in polymer electrolyte fuel cells, J. Power Sources **123**, 163–171 (2003)

19.157 A.B. Geiger, R. Eckl, A. Wokaun, G.G. Scherer: An approach to measuring locally resolved currents in polymer electrolyte fuel cells, J. Electrochem. Soc. **151**, A394–A398 (2004)

19.158 A. Hakenjos, C. Hebling: Spatially resolved measurement of PEM fuel cells, J. Power Sources **145**, 307–311 (2005)

19.159 I.A. Schneider, H. Kuhn, A. Wokaun, G.G. Scherer: Fast locally resolved electrochemical impedance spectroscopy in polymer electrolyte fuel cells, J. Electrochem. Soc. **152**, A2092–A2103 (2005)

19.160 A. Pozio, R.F. Silva, M. De Francesco, L. Giorgi: Nafion degradation in PEFCs from end plate iron contamination, Electrochimica Acta **48**, 1543–1549 (2003)

19.161 D.E. Curtin, R.D. Lousenberg, T.J. Henry, P.C. Tangeman, M.E. Tisack: Advanced materials for improved PEMFC performance and life, J. Power Sources **131**, 41–48 (2004)

19.162 S. Maass, F. Finsterwalder, G. Frank, R. Hartmann, C. Merten: Carbon support oxidation in PEM fuel cell cathodes, J. Power Sources **176**, 444–451 (2008)

19.163 H.-S. Oh, J.-G. Oh, S. Haam, K. Arunabha, B. Roh, I. Hwang, H. Kim: On-line mass spectrometry study of carbon corrosion in polymer electrolyte membrane fuel cells, Electrochem. Commun. **10**, 1048–1051 (2008)

19.164 M.S. Angelo, J. St-Pierre, K.P. Bethune, R.E. Rocheleau: Gas chromatography study of reactions of carbon monoxide at different operating temperatures within a PEMFC, Electrochem. Soc. Trans. **35**(32), 167–178 (2011)

19.165 E.A. Müller, F. Kolb, L. Guzzella, A.G. Stefanopoulou, D.A. McKay: Correlating nitrogen accumulation with temporal fuel cell performance, J. Fuel Cell Sci. Technol. **7**, 021013 (2010)

19.166 B.S. Pivovar: An overview of electro-osmosis in fuel cell polymer electrolytes, Polymer **47**, 4194–4202 (2006)

19.167 U. Beuscher: Experimental method to determine the mass transport resistance of a polymer electrolyte fuel cell, J. Electrochem. Soc. **153**, A1788–A1793 (2006)

19.168 J. St-Pierre, B. Wetton, G.-S. Kim, K. Promislow: Limiting current operation of proton exchange membrane fuel cells, J. Electrochem. Soc. **154**, B186–B193 (2007)

19.169 D.R. Baker, D.A. Caulk, K.C. Neyerlin, M.W. Murphy: Measurement of oxygen transport resistance in PEM fuel cells by limiting current methods, J. Electrochem. Soc. **156**, B991–B1003 (2009)

19.170 J. St-Pierre: Hydrogen mass transport in fuel cell gas diffusion electrodes, Fuel Cells **11**, 263–273 (2011)

19.171 A.J. Bard, L.R. Faulkner: *Electrochemical Methods: Fundamentals and Applications*, 2nd edn. (Wiley, New York 2001) pp. 335–353

19.172 Y. Garsany, O.A. Baturina, K.E. Swider-Lyons: Impact of sulfur dioxide on the oxygen reduction reaction at Pt/Vulcan carbon electrocatalysts, J. Electrochem. Soc. **154**, B670–B675 (2007)

19.173 Y. Garsany, O. Baturina, K.E. Swider-Lyons, S.S. Kocha: Experimental methods for quantifying the activity of platinum electrocatalysts for the oxygen reduction reaction, Anal. Chem. **82**, 6321–6328 (2010)

19.174 Y. Garsany, I.L. Singer, K.E. Swider-Lyons: Impact of film drying procedures on RDE characterization of Pt/VC electrocatalysts, J. Electroanal. Chem. **662**, 396–406 (2011)

19.175 D.A. Schiraldi: Perfluorinated polymer electrolyte membrane durability, Polym. Rev. **46**, 315–327 (2006)

19.176 M. Doyle, G. Rajendran: Perfluorinated membranes. In: *Handbook of Fuel Cells*, Vol. 3, ed. by W. Vielstich, A. Lamm, H.A. Gasteiger (Wiley, New York 2003) pp. 351–395

19.177 K.R. Cooper: Progress toward accurate through-plane ion transport resistance measurement of thin solid electrolytes, J. Electrochem. Soc. **157**, B1731–B1739 (2010)

19.178 Z. Siroma, T. Ioroi, N. Fujiwara, K. Yasuda: Proton conductivity along interface in thin cast film of Nafion, Electrochem. Commun. **4**, 143–145 (2002)

19.179 J. Li, K.G. Wilmsmeyer, L.A. Madsen: Anisotropic diffusion and morphology in perfluorosulfonate ionomers investigated by NMR, Macromolecules **42**, 255–262 (2009)

19.180 G. Velayutham: Effect of micro-layer PTFE on the performance of PEM fuel cell electrodes, Int. J. Hydrog. Energy **36**, 14845–14850 (2011)

19.181 D.J. Burnett, A.R. Garcia, F. Thielmann: Measuring moisture sorption and diffusion kinetics on proton exchange membranes using a gravimetric vapor sorption apparatus, J. Power Sources **160**, 426–430 (2006)

19.182 B. Ren, X.-B. Lian, J.-F. Li, P.-P. Fang, Q.-P. Lai, Z.-Q. Tian: Spectroelectrochemical flow cell with temperature control for investigation of electrocatalytic systems with surface-enhanced Raman spectroscopy, Faraday Discuss. **140**, 155–165 (2009)

19.183 R.J.K. Wiltshire, C.R. King, A. Rose, P.P. Wells, M.P. Hogarth, D. Thompsett, A.E. Russell: PEM fuel cell for in-situ XAS studies, Electrochimica Acta **50**, 5208–5217 (2005)
19.184 V. Croze, F. Ettingshausen, J. Melke, M. Soehn, D. Stuermer, C. Roth: The use of in-situ X-ray absorption spectroscopy in applied fuel cell research, J. Appl. Electrochem. **40**, 877–883 (2010)
19.185 M. Heinen, Z. Jusys, R.J. Behm: Ethanol, acetaldehyde and acetic acid adsorption/electrooxidation on a Pt thin film electrode under continuous electrolyte flow: An in-situ ATR-FTIRS flow cell study, J. Phys. Chem. C **114**, 9850–9864 (2010)
19.186 J.R. Anderson: *Structure of Metal Catalysts* (Academic, New York 1975)
19.187 L.A. Kibler, D.M. Kolb: Structure sensitive methods: AFM/STM. In: *Handbook of Fuel Cells*, Vol. 2, ed. by W. Vielstich, A. Lamm, H.A. Gasteiger (Wiley, New York 2003) pp. 266–278
19.188 R. Alink, D. Gerteisen, W. Mérida: Investigating the water transport in porous media for PEMFCs by liquid water visualization in ESEM, Fuel cells **11**, 481–488 (2011)
19.189 K.J.J. Mayrhofer, J.C. Meier, S.J. Ashton, G.K.H. Wiberg, F. Kraus, M. Hanzlik, M. Arenz: Fuel cell catalyst degradation on the nanoscale, Electrochem. Commun. **10**, 1144–1147 (2008)
19.190 Z.Y. Liu, J.L. Zhang, P.T. Yu, J.X. Zhang, R. Makharia, K.L. More, E.A. Stach: Transmission electron microscopy observation of corrosion behaviors of platinized carbon blacks under thermal and electrochemical conditions, J. Electrochem. Soc. **157**, B906–B913 (2010)
19.191 R.R. Adžić, J.X. Wang, B.M. Ocko, J. McBreen: EXAFS, XANES, SXS. In: *Handbook of Fuel Cells*, Vol. 2, ed. by W. Vielstich, A. Lamm, H.A. Gasteiger (Wiley, New York 2003) pp. 279–301
19.192 M.F. Mathias, J. Roth, J. Fleming, W. Lehnert: Diffusion media materials and characterisation. In: *Handbook of Fuel Cells*, Vol. 3, ed. by W. Vielstich, A. Lamm, H.A. Gasteiger (Wiley, New York 2003) pp. 517–537
19.193 N.L. Garland, J.P. Kopasz: The United States Department of Energy's high temperature, low relative humidity membrane program, J. Power Sources **172**, 94–99 (2007)
19.194 E.D. Wachsman, K.T. Lee: Lowering the temperature of solid oxide fuel cells, Science **334**, 935–939 (2011)